Testing Hydrogen admixture for Gas Applications

Non-combustion related impact of hydrogen admixture - material compatibility

Deliverable: D2.4
Status: Final, 24th of June 2020
Dissemination level: Public

The THyGA project has received funding from the Fuel Cells and Hydrogen Joint Undertaking under grant agreement No. 874983. This Joint Undertaking receives support from the European Union's Horizon 2020 research and innovation programme, Hydrogen Europe and Hydrogen Europe research.

Document classification

Title	Non-combustion related impact of hydrogen admixture - material compatibility
Deliverable	D2.4
Reporting Period	M6
Date of Delivery foreseen	M6
Draft delivery date	M5
Validation date	M6

Authors	Lisa Blanchard[1], Laurent Briottet[1]
Affiliation	[1] CEA, Grenoble, France
Corresponding authors	Lisa Blanchard, lisa.blanchard@cea.fr Laurent Briottet, laurent.briottet@cea.fr

Work package	WP 2
Dissemination	PU = Public
Nature	Report
Version	Final version
Doc ID Code	THY_WP2_001_Literature review Task 2.4_v4.1
Keywords	Hydrogen embrittlement, Leakage, Permeation, Metallic materials, Polymers

Document History

Partner	Remark	Version	Date
CEA	Draft	1	04th May, 2020
CEA	Amendments and consolidation from GWI and ENGIE partners feedback	2	18th June, 2020
CEA	Finalisation	Final	24th June, 2020

Document review

Partner	Approval
ENGIE	Patrick Milin (patrick.milin@engie.com)
GWI	Johannes Schaffert (schaffert@gwi-essen.de), Jörg Leicher (leicher@gwi-essen.de)

Acknowledgements

The authors would like to express their thanks to Johannes Schaffert (GWI), Jörg Leicher (GWI) and Patrick Milin (ENGIE) for their insights, comments and reviews. Mustafa Flayyih (GWI) is also thanked for his help in providing data on acceptable leaking rates for gas distribution components.

Executive summary

The present document is part of a larger literature survey of this WP, aiming to establish the current status of gas utilisation technologies in order to determine the impact of hydrogen (H_2) admixture on natural gas (NG) appliances. This part focuses on the non-combustion related aspects of injecting hydrogen in the gas distribution networks within buildings, including hydrogen embrittlement of metallic materials, chemical compatibility and leakage issues.

In the particular conditions of adding natural gas and hydrogen (NG / H_2) mixture into a gas distribution network, hydrogen is likely to reduce the mechanical properties of metallic components. This is known as hydrogen embrittlement (HE) (Birnbaum, 1979). This type of damage takes place once a critical level of stress / strain and hydrogen content coexist in a susceptible microstructure. Currently, four mechanisms were identified and will be discussed in detail. The way those mechanisms act, independently or together, is strongly dependent on the material, the hydrogen charging procedure and the mechanical loading type. The main metallic materials used in gas appliances and gas distribution networks are: carbon steels, stainless steels, copper, brass and aluminium alloys (Thibaut, 2020). The presented results showed that low alloy steels are the most susceptible materials to hydrogen embrittlement followed by stainless steels, aluminium, copper and brass alloys. However, the relative pressures of the operating conditions of gas distribution network in buildings, are low i.e. between 30 to 50 mbar. At those low hydrogen partial pressures, it is assumed that a gas mixture composed of NG and up to 50% H_2 should not be problematic in terms of HE for any of the metallic materials used in gas distribution network, unless high mechanical stress / strain and high stress concentrations are applied.

The chemical compatibility of hydrogen with other materials, and specifically polyethylene (PE) which is a reference material for the gas industry, is also discussed. PE was found to have no corrosion issues and no deterioration or ageing was observed after long term testing in hydrogen gas.

The last non-combustion concern related to the introduction of hydrogen in natural gas distribution network is the propensity of hydrogen toward leakage. Indeed, the physical properties of hydrogen are different from other gases such as methane or propane, and it was observed that hydrogen leaks 2.5 times quicker than methane.

This bibliographical report on material deterioration, chemical compatibility and leakage concerns coming with the introduction of NG / H_2 mixture in the gas distribution network sets the basis for the upcoming experimental work where the tightness of gas distribution network components will be investigated (Task 3.2.3 WP3). In addition, tightness of typical components that connect end-user appliances to the local distribution line shall be evaluated as well.

List of abbreviations

BCC	Body-centred cubic
FCC	Face-centred cubic
HCP	Hexagonal close packed
HE	Hydrogen Embrittlement
HEDE	Hydrogen Enhanced Decohesion Embrittlement
HELP	Hydrogen Enhanced Localised Plasticity
HESIV	Hydrogen Enhanced Strain-Induced Vacancies
HIC	Hydrogen Induced Cracking
HID	Hydrogen Induced Decohesion
HTHA	High Temperature Hydrogen Attack
IG	Intergranular
J value	A method for measuring the material fracture toughness. The critical value J_{1C} is linked to the critical energy for a given crack to propagate.
NG	Natural Gas
NG / H_2	Natural Gas / Hydrogen blend
PE	Polyethylene

Table of contents

1 Introduction

The present document is part of a larger literature survey of this WP aiming to establish the current status of gas utilisation technologies in order to determine what would be the impact of hydrogen admixture on gas appliances. This part focuses on the non-combustion related aspects of injecting hydrogen in the gas distribution network, including hydrogen embrittlement and leakage issues.

Hydrogen can reduce the mechanical properties of metallic materials in different ways depending on the material, the temperature and the hydrogen charging conditions (*Mechanics - Microstructure - Corrosion Coupling - 1st Edition*, 2019). For example, at temperatures around 400°C, steels submitted to hydrogen pressure may experience high temperature hydrogen attack (HTHA): bubbles of methane appear in the core of the material, leading to failure.

At room temperature in a sour environment (containing H_2S), hydrogen induced cracking (HIC) can occur: bubbles of hydrogen gas are formed around carbides and increase of the hydrogen pressure in the void will eventually lead to material blistering. Some metals, such as titanium or zirconium alloys, subjected to high hydrogen charging conditions will be embrittled by the formation of hydrides.

This project is concerned with addressing the distribution and use of NG / H_2 mixtures around room temperature. In those particular conditions, hydrogen is likely to reduce the mechanical properties of metals by other mechanisms known as hydrogen embrittlement (HE) (Birnbaum, 1979). This takes place once a critical level of stress / strain and hydrogen content coexist in a susceptible microstructure.

Currently, several mechanisms are proposed and discussed. The first part of this work will focus on the hydrogen susceptibility of the main materials used in gas appliances and gas distribution network: carbon steels, stainless steels, copper, brass, aluminium alloys and polyethylene (Thibaut, 2020). In a second part, the chemical compatibility of hydrogen with other materials is discussed with the propensity of hydrogen toward leakage in metallic and polymer materials.

2 Hydrogen embrittlement

2.1 Generalities

HE has been an issue for many years across diverse industry sectors since it drastically reduces mechanical properties of a large range of metallic materials. As hydrogen ingresses into a susceptible material, ductility is decreased which can induce cracking and failures at stresses below the yield stress. In a hydrogen gas environment at room temperature, the dihydrogen molecule (H_2) dissociates and each atom is adsorbed at the metal surface. If the hydrogen atoms do not recombine and are absorbed by the bulk material, they diffuse through the crystal lattice. Transport of hydrogen within a material is a combination of diffusion and solubility, whose properties are highly dependent on the type of crystallographic microstructure. Body-centred cubic (BCC) crystallographic microstructures, such as ferritic steels, have higher hydrogen diffusion coefficients than face-centred cubic (FCC) ones (Birnbaum and Wert, 1972). Typically, the hydrogen diffusion coefficient is five orders of magnitude higher in ferrite than in austenite: $D_{ferrite} \approx 10^{-11}$ $m^2.s^{-1}$ and $D_{austenite} \approx 10^{-16}$ $m^2.s^{-1}$. On the other hand, the solubility is higher in FCC than in BCC microstructures, typically $S_{ferrite} = 2{,}6 \times 10^{-4}$ ppm by mass and $S_{austenite} = 0{,}35$ ppm by mass at 20°C under 1 atm H_2 (Brass et al., 2000). In the metal, the H interstitial sites are the tetragonal sites in the BCC microstructure and the octahedral sites in the FCC one, Figure 1.

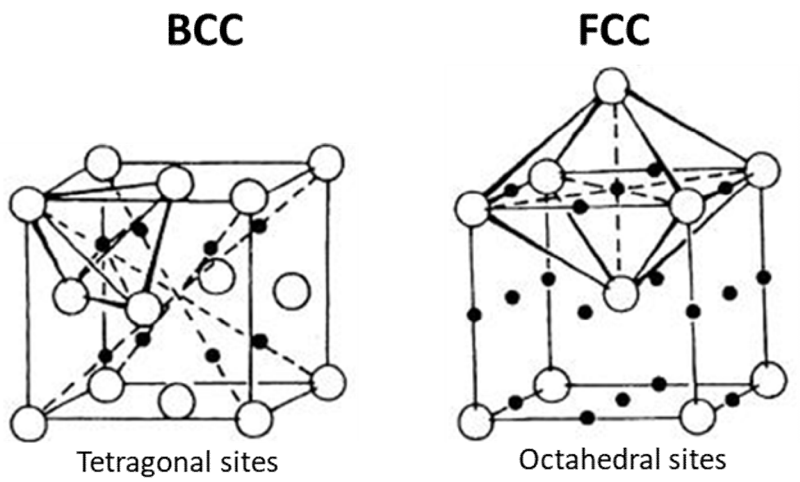

Figure 1 : Interstitial trapping sites in bcc and fcc crystallographic structures (Fukai, 2005).

Many questions remain to explain how hydrogen leads to such losses of properties. Four main mechanisms have been proposed, each of them being preponderant depending on the material, H environment and loading conditions. They are presented below.

2.2 Proposed mechanisms for hydrogen embrittlement

The main mechanisms currently accepted, under hydrogen pressure and around room temperature, consider decohesion of the lattice plane or of interfaces (HEDE: Hydrogen Enhanced Decohesion or HIP: Hydrogen Induced Decohesion), hydrogen – dislocations interactions (HELP: Hydrogen Enhanced Localised Plasticity and AIDE: Adsorption Induced Dislocations Emission) and hydrogen – vacancies interactions (HESIV: Hydrogen-enhanced stress-induced vacancy).

2.2.1 Decohesion models: HEDE or HID

HEDE (Hydrogen Enhanced Decohesion), also found in the literature as HID (hydrogen induced decohesion) assumes that hydrogen weakens the atomic cohesive bond between atoms, grain boundaries, matrix/precipitates interfaces, as described in Figure 2 (Lynch, 2011; Oriani and Josephic, 1974; Pfeil, 1926). Computer simulation techniques have been used to demonstrate the evolution of cohesive strength with hydrogen pressure (Song *et al.*, 2010), Figure 3 a). This theory suggests that resulting fracture surfaces would exhibit 100% of intergranular fracture or cleavage. If this has been observed under particular hydrogen charging and strain conditions (Oriani and Josephic, 1974), however, what is most commonly observed on fractographies is a mixed mode of intergranular features (IG) (Li et al., 2018) and quasi-cleavage: a combination of brittle facets surrounded by plastically sheared areas. Thus, this mechanism cannot explain the observed fracture surfaces, and the occurrence of additional fracture mechanisms is necessary.

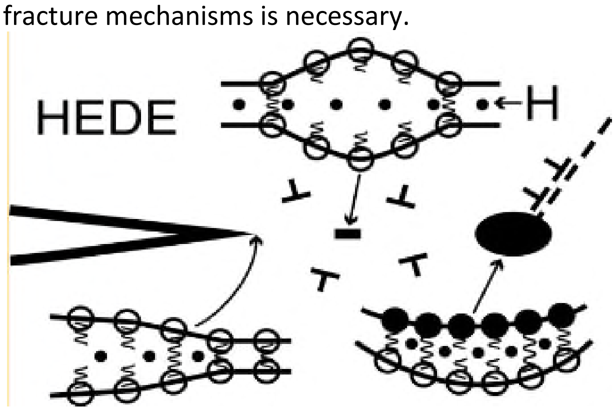

Figure 2 : Scheme of the HEDE mechanism (Lynch, 2011).

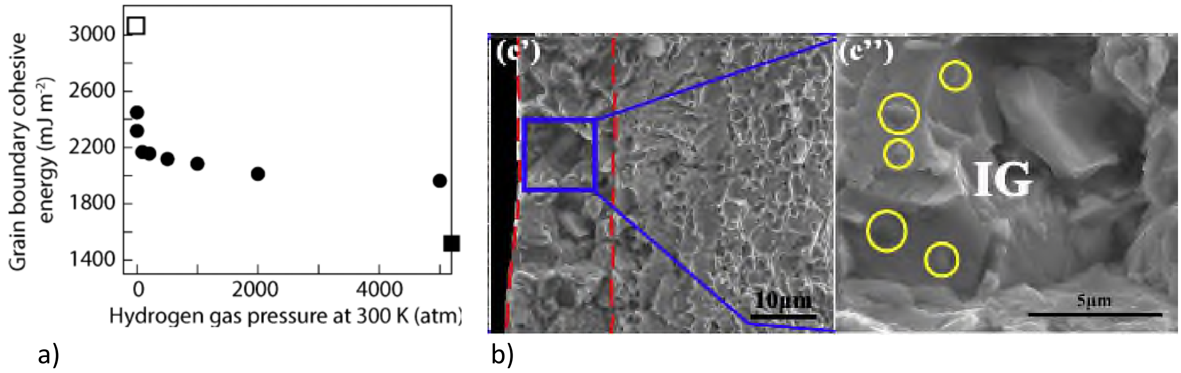

Figure 3 : a) Grain boundary cohesive energy as a function of hydrogen pressure for a Fe grain boundary. Open square: no hydrogen and filled squares-gas pressure of 5GPa (Wang et al., 2015), (Robertson et al., 2015), b) Fracture surface of an uniaxial tensile specimen of IN718 alloy hydrogen pre-charged by electrochemical method and tested under cathodic charging exhibiting intergranular (IG) areas. The yellow circles represent tearing ridges on grain boundaries(Li et al., 2018).

2.2.2 Hydrogen - Plasticity related models: AIDE and HELP

On the opposite of HEDE, the HELP (Hydrogen Enhanced Localised Plasticity) and AIDE (Adsorption Induced Dislocations Emission) models are related to plasticity. The HELP mechanism assumes that once hydrogen ingresses within the material at crack tip or highly stressed regions in the material, it creates shielding around dislocations and obstacles, reducing the strength of their internal stress field and hence, facilitating their mobility (Birnbaum and Sofronis, 1994), (Abraham and Altstetter, 1995; Lynch, 2012). This local increase of dislocations mobility induces local slip, leading to microvoid-coalescence (mvc) more localised than in inert environment (Abraham and Altstetter, 1995). Thus, the macroscopic loss of ductility is due to a strong localization of plastic deformation. The resulting fracture surfaces exhibits a mixture of quasi-cleavage and ductile micro void coalescence (Nagao *et al.*, 2014).

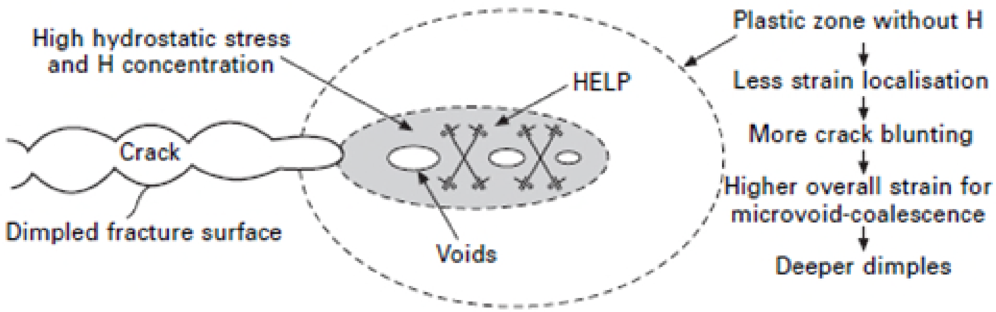

Figure 4 : Scheme of the HELP mechanism (Lynch, 2011).

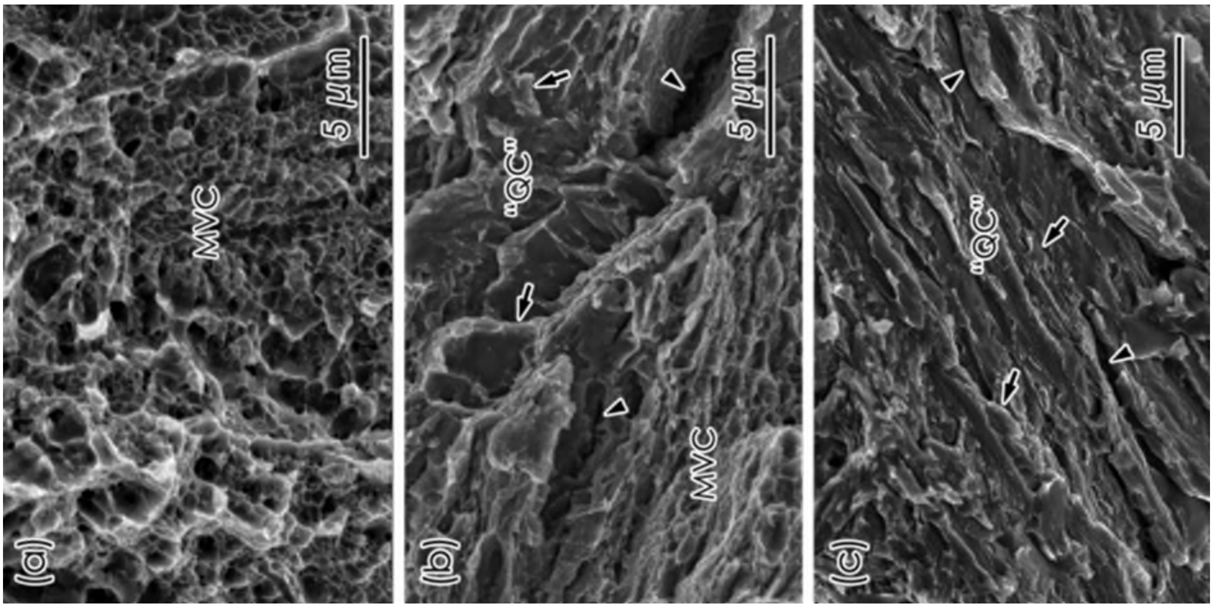

Figure 5 : Fracture surfaces of Steel-B550 for a) uncharged specimen, b) hydrogen charged specimen in 31 MPa hydrogen gas and c) hydrogen charged specimen exposed to 138 MPa hydrogen gas. QC: quasi-cleavage and MVC: micro void coalescence.

The AIDE model is also based on hydrogen – dislocations interactions but focuses on the metal surface facing the gas. Figure 6, is a representation of the AIDE model, whereby it is assumed that chemisorption of hydrogen facilitates the nucleation of dislocations in strained area, such as crack tip. This phenomenon implies that in the plastic zone ahead of the crack tip, the general dislocation activity is eased leading to nucleation and growth of voids at slip-band intersections, inclusions, second-phase particles... and hence, further crack propagation.

Both HELP and AIDE mechanisms are based on hydrogen – plasticity interactions, HELP on the bulk material whereas AIDE is a surface related mechanism.

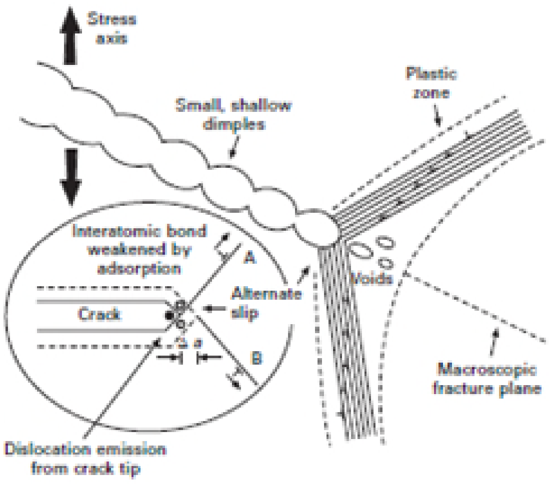

Figure 6 : Scheme of AIDE mechanism (Lynch, 2011).

2.2.3 Hydrogen interaction with vacancies: HESIV

Hydrogen-enhanced stress-induced vacancy (HESIV) is a mechanism whereby hydrogen enhances the formation of vacancies under plastic straining inducing a reduction of ductile crack growth resistance (Nagumo, 2004). The increase of vacancy density generates either the formation of microvoids formation or an amorphization of the fracture subsurface. Nagumo *et al.* (Takai *et al.*, 2008), found that under straining, hydrogen damages the material in an irreversible manner. Figure 7 gives the results of their work in which iron specimens were strained in hydrogen environment up to a point where hydrogen was removed and the test terminated in air. It was observed that the material does not recover its full mechanical properties after removing hydrogen at a late stage of straining. This is a strong argument for hydrogen enhancing the creation of strain-induced defects and explaining the irreversibility of the observed results.

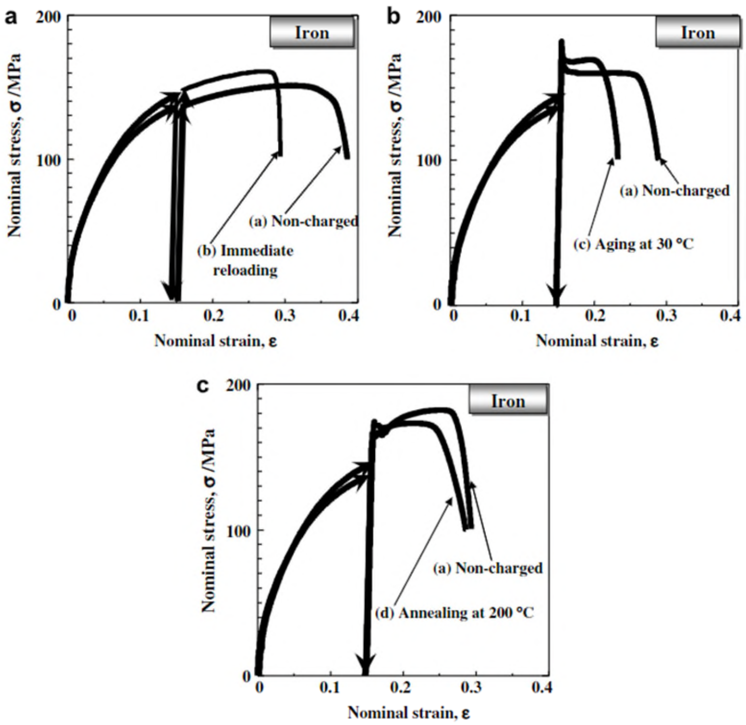

Figure 7 : Stress strain curves of hydrogen-charged iron a) immediate reloading after interposed unloading, b) aging at 30°C for 168 h at the unloaded stage and c) annealing at 200°C for 2 h at the unloaded stage (Takai et al., 2008).

2.2.4 Summary

Hydrogen embrittlement has been studied since 1874 (Johnson, 1874) and through investigations and with the progress in experimental techniques, many mechanisms were proposed. Currently, the four mechanisms presented are the ones remaining, which have not been ruled out by experiment. However, it is unclear if one is predominant, if they are acting together and if so, how they interact together (Dadfarnia *et al.*, 2015b; Djukic *et al.*, 2014). This is also strongly dependent on the material, the hydrogen charging procedure and loading type.

Currently, mechanisms are described independently, however due to the interdependence of the factors acting in the hydrogen embrittlement process of a material, the overall mechanism is still not fully understood.

2.3 Influencing factors

As presented in the introduction, HE is a mechanism occurring from the coexistence of a critical level of hydrogen and strain/stress fields in a susceptible microstructure. Those parameters being interdependent, an increase of hydrogen concentration in a particular alloy microstructure may reduce the strain level required for failure to occur. In the following, the main effects of these different parameters are discussed.

2.3.1 Material

This section gives an overview on how material parameters influence the susceptibility to hydrogen. The main materials employed in gas appliances are described in the following section.

The microstructure plays a critical role on the susceptibility to HE of an alloy Table 1 give a classification of the susceptibility of the microstructures. Those differences are explained by the fact that hydrogen transport, diffusion and solubility are dependent on the crystallographic structure: BCC, FCC, hexagonal close packed (HCP) of the alloy. Liu et al. investigated the influence of the austenite fraction in Mn-steels: as the austenitic fraction get more stable and its fraction increased, the hydrogen diffusion decreased (Liu *et al.*, 2020). Furthermore, it is clear that the reduction of residual micro-stresses in the microstructure using tempering have a beneficial effect on the susceptibility to HE (Luppo and Ovejero-Garcia, 1991).

Table 1 : Observed trend on the microstructure susceptibility to HE for a given level of mechanical properties

Most susceptible microstructure	**Order of increasing the resistance to HE** →			**Less susceptible microstructure**	**References**
Martensitic materials	Ferritic materials			Stable austenitic alloys	(Barthelemy, 2006)
Ferritic/perlitic			Tempered bainite		(Brass *et al.*, 2000)
Martensite	Bainite	Perlite	Tempered bainite	Tempered martensite	(“FD E29-649 Bouteilles à gaz transportables - fragilisation par l’hydrogène des aciers,” 2016)

Particular sites in alloy microstructures act as traps for hydrogen, resulting in a higher concentration of hydrogen at those locations. Those sites are mainly lattice imperfections such as inclusions, particles, phase interfaces, grain boundaries (GB), secondary phases, vacancies and dislocations (Luppo and Ovejero-Garcia, 1991), (Liu *et al.*, 2019). The presence of those sites can have a detrimental effect by acting as crack initiation, but they can also act as hydrogen tank, lowering hydrogen activity in the alloys and hence being advantageous.

Depending on the nature of the alloy, a passive film of oxide can develop at the metal surface. It was found this oxide layer acts as a barrier for hydrogen to ingress in the material reducing the effective hydrogen diffusion coefficient (Bruzzoni and Riecke, 1994), (Legrand *et al.*, 2012).

2.3.2 Loading conditions

The presence of internal or external stress and strain influences hydrogen transport and distribution in the microstructure. Indeed, hydrogen concentrates at lattice distortion induced by stress: concentration factor such as crack tip in fracture toughness specimens, phases with higher level of residual stresses induced by manufacturing processes (Kirchheim, 1986). Furthermore, during testing, HE susceptibility increases with decreasing strain rate (Lynch, 2011), (Ez-Zaki *et al.*, 2018) this is thought to be due to hydrogen diffusion having more time to occur at low stain rates.
The two following equations show how the diffusion and solubility are influenced by external stress:

$$\underbrace{\frac{D}{Deff}\frac{\partial C_L}{\partial t}}_{\text{Trapping}}+\alpha\theta_T\underbrace{\frac{dN_T}{d\varepsilon^p}}_{\substack{\text{Hydrogen trapping}\\\text{by the dislocations}\\\text{trapping}}}\frac{d\varepsilon^p}{dt}\underbrace{-D\nabla^2 C_L}_{\substack{\text{Lattice}\\\text{diffusion}}}+\underbrace{\nabla\left(\frac{DV_H}{3RT}C_L\nabla\sigma_{kk}\right)}_{\substack{\text{Diffusion induced}\\\text{by stress}}}+\underbrace{\nabla\left(\alpha\theta_T N_T^m V^d\right)}_{\substack{\text{Hydrogen}\\\text{transport by the}\\\text{dislocations}}}=0 \qquad \textit{Equation 1}$$

Where D_{eff} is the effective diffusion coefficient, C_L the concentration of the interstitial lattice sites, N_T the dislocation trap density, θ_T is the trapping sites occupancy, ε^P is the effective plastic strain, σ_{kk} is the trace of the stress tensor, α is the number of trapping sites per dislocation trap, T is the temperature and R the gas constant (Dadfarnia *et al.*, 2015a).

$$\frac{S}{S_0} = \exp\left[\frac{\sigma_m V_H}{K_B T}\right] \qquad \textit{Equation 2}$$

with K_B Boltzmann's constant, V_H partial molar volume (~2 $cm^3.mol^{-1}$) (Krom, 1998), (Krom *et al.*, 1999). Hence, stress and strain influence hydrogen distribution and transport in the material microstructure, and hydrogen influences stresses and plasticity in the material which leads to embrittlement, as described in the previous sections.

2.3.3 Hydrogen charging conditions

When testing materials under gaseous hydrogen, an increase in hydrogen-gas pressure results in increasing HE susceptibility (Lynch, 2011). Figure 8 shows results obtained after fatigue crack growth testing of an ARMCO iron under 35 MPa and 3.5 MPa hydrogen pressure. As hydrogen pressure increases, the susceptibility to HE increases as well.

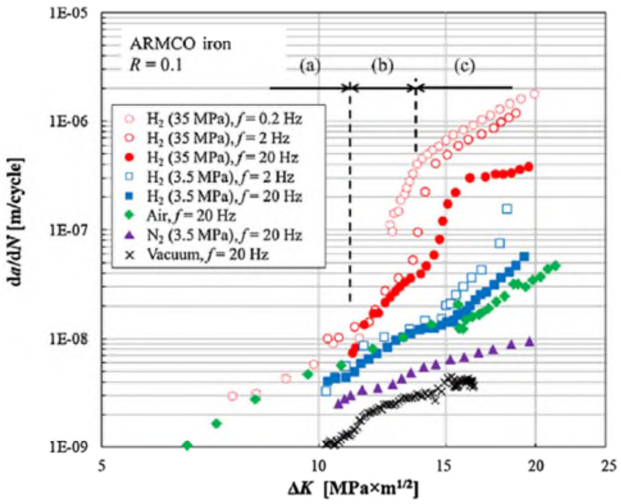

Figure 8 : Fatigue crack growth curves obtained for an Armco iron tested under different hydrogen pressure and testing frequencies (Shinko et al., 2019).

It is around ambient temperature that the most detrimental effect of HE was observed. At lower temperatures, both hydrogen diffusion and solubility decrease, reducing the effect of hydrogen, while at higher temperatures alloys have more ductile properties preventing this type of embrittlement.

In the context of evaluating material suitability for transporting hydrogen gas mixture, it was observed that the presence of impurities in the gas could inhibit or facilitate HE to occur (Ez-Zaki *et al.*, 2018). Indeed, it was found that O_2 inhibits dihydrogen dissociation and hence, H ingress in the material and has an effect at very low concentration (0.1 vppm) (Komoda *et al.*, 2019), whereas H_2S facilitates this entrance (Fukuyama and Yokogawa, 1990), water vapour however, could have beneficial or detrimental effect, depending on the alloys. Figure 9 illustrates the influence of various compounds on the fatigue crack growth resistance of 2.25r-1Mo steel. The results are given according to $(da/dn)_{inhibitor}$ $/(da/dn)_{hydrogen}$, with da/dn the fatigue crack rate.

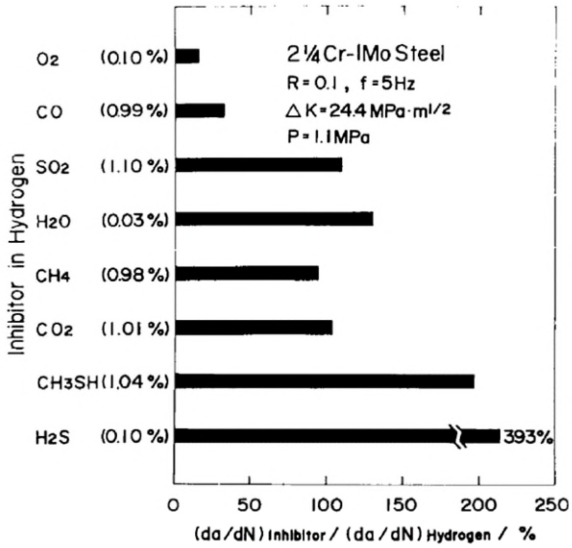

Figure 9: Effect of gas inhibitors added to 1.1 MPa hydrogen on fatigue 2.25r-1Mo steel under ΔK of 24 MPa.m$^{1/2}$ a room temperature (Fukuyama and Yokogawa, 1990).

2.4 Susceptibility of metallic materials used in gas appliances towards hydrogen embrittlement

The last part of this section focuses on the susceptibility to hydrogen embrittlement of the main metallic materials used on the distribution gas network and appliances components: carbon steels, stainless steels, copper, aluminium and brass.

2.4.1 Carbon steels

Many studies, investigating the action of hydrogen gas on carbon steel, have observed a loss of ductility (Capelle *et al.*, 2008), (Briottet and Ez-Zaki, 2018, p. 70), (Nguyen *et al.*, 2020), toughness (Wang, 2009), (Yang *et al.*, 2015) and a decrease of the fatigue life (Marrow *et al.*, 1992), (San Marchi and Somerday, 2012).

The following figures show the resulting loss of mechanical properties obtained in order to evaluate service life of carbon steel components in hydrogen gas at room temperature (Briottet *et al.*, 2012). Figure 10 displays tensile curves for a X80 steel tested in air, nitrogen and hydrogen environment at 300 bar. A clear loss of ductility was observed, obtained in hydrogen compared to the one in air and nitrogen. The Figure 11 displays typical fracture faces of steel tested in air and in hydrogen at 10 MPa. The characteristic embrittlement induced by hydrogen was observed: absence or reduction of necking of the specimen, sharp secondary cracks developing and quasi-cleavage.

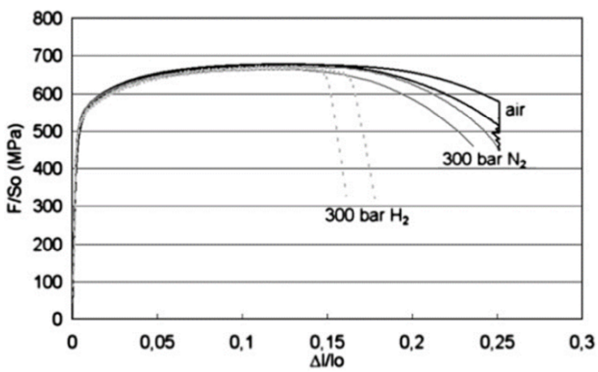

Figure 10 : Tensile test results obtained for specimens extracted from a X80 steels and tested in air, in 300 bar nitrogen and in 300 bar hydrogen (Briottet et al., 2012).

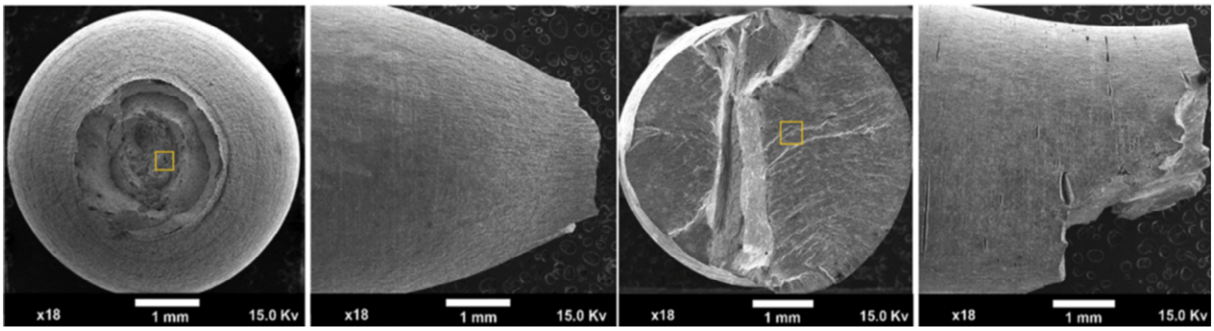

a) b)

Figure 11 : Fractography images of X70 pipeline steel tested a) in air and b) in 10 MPa hydrogen (Nguyen et al., 2020).

HE susceptibility is highly dependent on the type of mechanical loading and stress distribution. The presence of a defect, such as a crack, induces a concentration of stresses ahead of the crack tip, which enhances the increase of hydrogen concentration locally (Kirchheim, 1986). This was demonstrated in Nguyen *et al.* work (Nguyen *et al.*, 2020) in which the HE susceptibility was evaluated in a mixture of natural gas and 1% H_2 at 10 MPa. Under these conditions, tensile properties of smooth specimens were not affected while fracture toughness properties were clearly reduced. The J-R curve (Briottet *et al.*, 2012), Figure 12 b), showed that in hydrogen gas environment at 300 bar pressure, the X80 steel exhibited a low resistance with a J integral value inferior to 25 kJ/m² at a crack advance close to 0.45 mm, estimated at $J_{0.2}$ = 0.2 mm. From this decrease in fracture toughness properties, a defect acceptance criterion was estimated. The simulation showed that defects only 2 to 3 times smaller than in natural gas could be accepted (Briottet *et al.*, 2012). Loss of crack resistance was also observed on a X70 steel in N_2 / H_2 mixture up to 1% H_2 at 85 bar, Figure 13 (Briottet and Ez-Zaki, 2018).

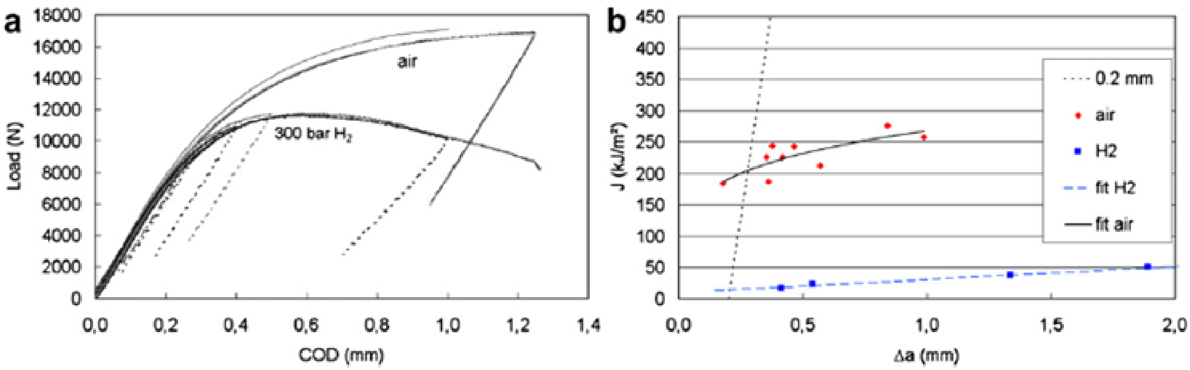

Figure 12 : Toughness test results obtained for specimens extracted from a X80 steel in air, in 300 bar nitrogen and in 300 bar hydrogen a) load vs crack opening displacement curves, b) J-R curves (Briottet et al., 2012).

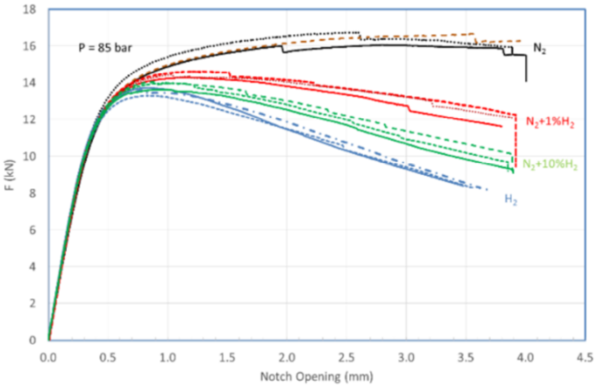

Figure 13 : Influence of hydrogen content in a N_2 / H_2 gas mixture on load crack opening curves (Briottet and Ez-Zaki, 2018).

Figure 14 is an example of the increase of fatigue crack growth rate obtained in hydrogen environment compared to air for pure iron. The figure also demonstrates the influence of the gas pressure, the fatigue crack growth rate highly accelerated with the pressure test going from 0.7 to 90 MPa. For those low alloyed steels, acceleration of crack growth rate from 30 to 100 times in hydrogen environment compared to air is classically observed. Figure 14 shows that, depending on the hydrogen pressure, there is a stress intensity factor under which crack growth rate in hydrogen is similar to the one in air.

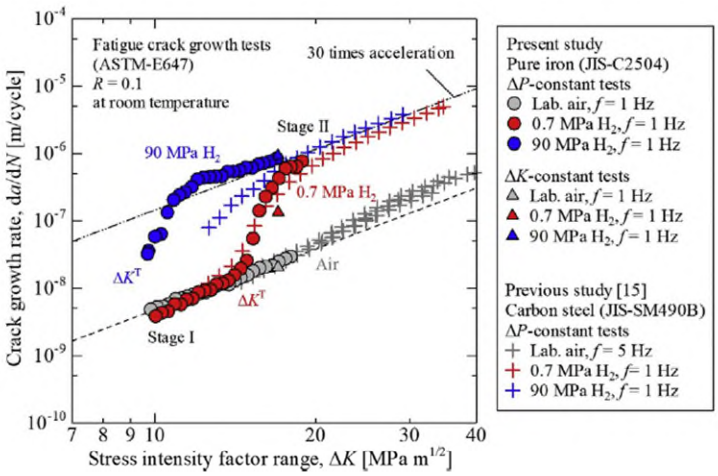

Figure 14 : Fatigue crack growth results obtained in air and in hydrogen environments at 0.7 MPa and 90 MPa for pure iron and carbon steel materials (Birenis et al., 2018).

2.4.2 Stainless steels

Experience has shown low alloy steels are more susceptible to HE than stainless steels (San Marchi and Somerday, 2012). The previous section on the factors influencing the resistance to HE has described that ferritic stainless steels (SS) are generally more affected than austenitic stainless steels by HE. Table 2 gives the tensile test results of several ferritic and austenitic SS in air, in helium and in hydrogen environments (San Marchi and Somerday, 2012). The higher susceptibility to HE of ferritic SS was observed with a stronger decrease in elongation and reduction area in hydrogen environment compared to the austenitic SS.

Table 2 : Tensile properties of smooth tensile specimens extracted for ferritic (FSS) and austenitic stainless steels (ASS) (San Marchi and Somerday, 2012).

	Material	Test environment	Strain rate, s^{-1}	Yield strength, MPa	Ultimate strength, MPa	El, %	RA, %	Ref
FSS	Annealed 430F, heat treat W69	69 MPa He 69 MPa H_2	0.67 $\times 10^{-3}$	496	552 538	22 14	64 37	(Jewett *et al.*, 1973)
ASS	316, cold drawn heat W69	69 MPa He 69 MPa H_2	0.67 $\times 10^{-3}$	441	648 683	59 56	72 75	(Jewett *et al.*, 1973)
	Annealed sheet	Air 70 MPa He 70 MPa H_2	0.6 $\times 10^{-3}$	263 248 249	568 565 566	90 85 85	75 70 75	(Vandervoort and Raymond, 1976)
	304L, heat treat W69 annealed	69 MPa He 69 MPa H_2	0.67 $\times 10^{-3}$	234	531 524	86 79	78 71	(Jewett *et al.*, 1973)
	304L	Air 69 MPa He 69 MPa H_2		186 186 220	530 565 503	73 74 33	77 81 32	(Louthan *et al.*, 1972)

However, many different grades of austenitic alloys exit, some of each having lower austenitic phase stability and experiencing martensitic transformation under straining. Those grades are found more susceptible to HE than the ones with stable austenitic phase (Eliezer *et al.*, 1979), (Perng and Altstetter, 1987). Figure 15 illustrates this effect: notched specimens of two austenitic (AISI 301 and AISI 310) and a ferritic (AL 29-4-2) stainless steels were tested in hydrogen environment (1.08 bar) (Perng and Altstetter, 1987). The results show that the AISI 310, which does not undergo martensitic transformation, exhibited higher HE resistance than the two other alloys. It was also observed as the temperature increased the effect of hydrogen embrittlement was reduced. No effects were observed up above 150°C. Figure 16 presents the fracture surfaces obtained for the AISI 301 and AL 29-4-2 grades. Both exhibited quasi-cleavage characteristic of HE and intergranular cracking for the AISI 301 (Perng and Altstetter, 1987).

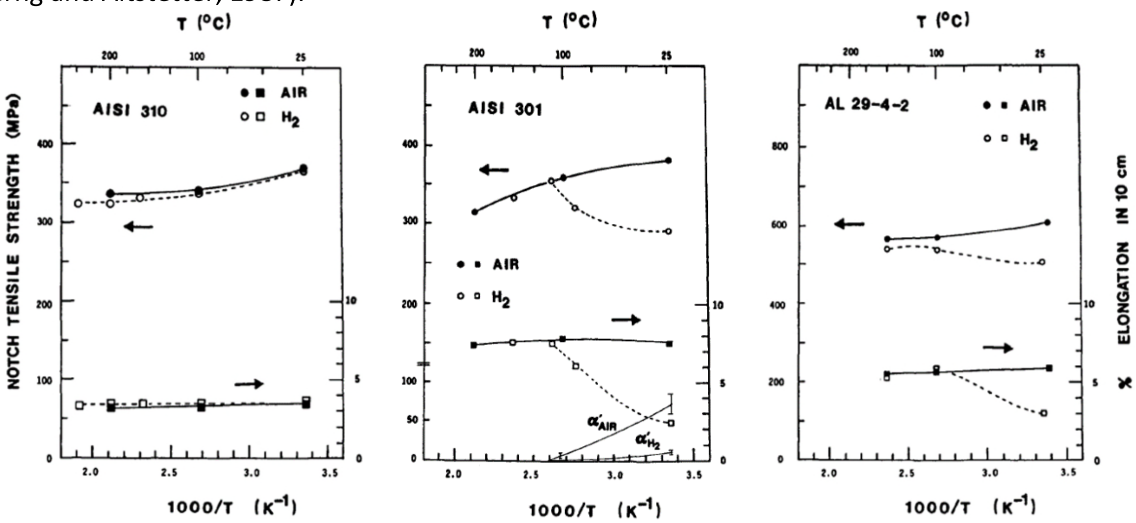

a) b) c)

Figure 15: Notch tensile strength results of a) the austenitic AISI 310 alloy, b) the austenitic AISI 301 alloy, and c) the ferritic Al 29-4-2 tested in air and 108 kPa H_2 pressure at 25°C to 200°C under 108kPa H_2 gas pressure (Perng and Altstetter, 1987).

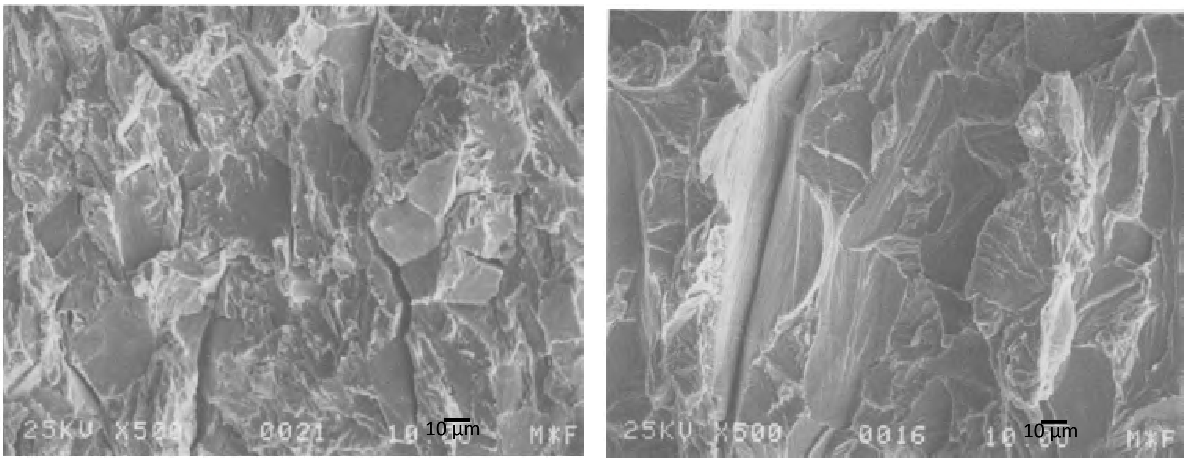

a) b)

Figure 16 : Fractographies of a) the austenitic AISI 301 alloy and b) the ferritic Al 29-4-2 tested at 25°C under 108kPa H_2 gas pressure (Perng and Altstetter, 1987).

2.4.3 Copper and copper alloys

Very few data are available in the literature on the susceptibility of copper alloys to HE, but it is generally considered that their susceptibility to HE is low: closed to the one of aluminium and austenitic stainless steel alloys (Louthan and Caskey, 1976), (Jewett *et al.*, 1973). The European project GRHYD has tested the resistance to HE of pure copper smooth and notched tensile specimens in three (GN + H_2) gas admixtures, with H_2 content being 6%, 20% and 50% (Briottet and Portra, 2017). In those conditions, no influence of hydrogen was observed, Figure 17.

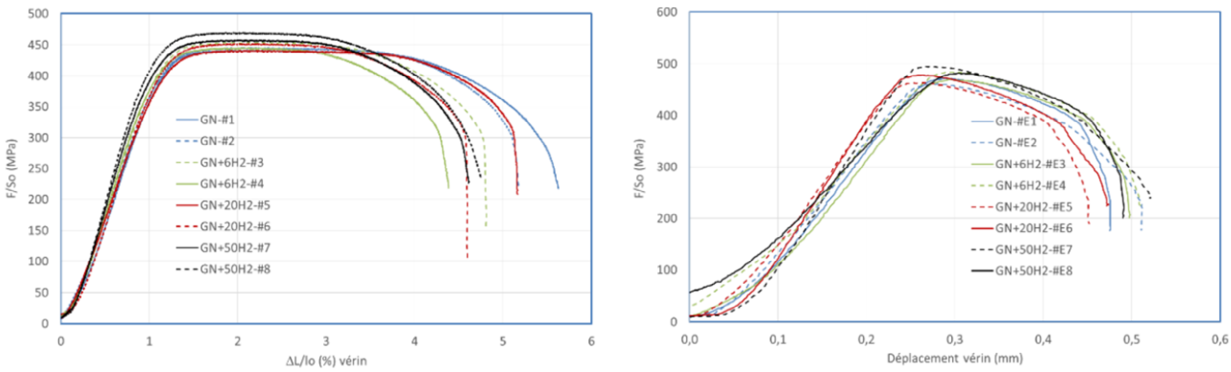

a) b)

Figure 17 : Tensile curves results for pure coper alloy on a) smooth and b) notched specimens (Briottet and Portra, 2017).

A type of copper alloys is the OFHC (oxygen free high conductivity) in which the absence of oxygen is assessed using hydrogen gas at elevated temperature. If oxides are present in the microstructure, they are located at grain boundaries and they react with hydrogen, creating water vapour bubbles, which can lead to blistering. This type of embrittlement is similar to the recombination of hydrogen causing blistering in steels (San Marchi and Somerday, 2012), (Jewett *et al.*, 1973; Nieh and Nix, 1980) but is only used as assessment for OFHC and this testing is far from operating conditions in which those alloys are used.

2.4.4 Aluminium alloys

Aluminium (Al) alloys have a FCC crystallographic structure, inducing low hydrogen diffusion properties, in the order of austenitic or nickel alloys. Furthermore, Al alloys have the particularity to be covered by a very stable oxide film in all reducing environments. Due to this film, the dihydrogen molecule (H_2) does not dissociate which impedes the adsorption of hydrogen atoms within the bulk material, reducing the permeation properties. A way of introducing hydrogen within Al is the introduction in an environment where hydrogen atoms are readily present, such as water vapour or cathodic charging (Scully *et al.*, 2012). In those environments, the HE susceptibility of Al has been extensively studied and the reduction of ductility due to hydrogen was observed (Ambat and Dwarakadasa, 1996; Bond *et al.*, 1988; Dey and Chattoraj, 2016; Kamoutsi *et al.*, 2006; Panagopoulos and Papapanayiotou, 1995). In dry hydrogen however, no reduction of toughness and ductility was observed (Louthan and Caskey, 1976), (San Marchi and Somerday, 2012).

2.4.5 Brass

The literature on the susceptibility of hydrogen in brass is not extensive. Panagoloupos *et al.* (Panagopoulos *et al.*, 2005) have studied the influence of hydrogen on a 70 wt.% Cu–30 wt.% Zn. Severe cathodic charging in the presence of a poisoning agent were used to introduce hydrogen into the material, resulting in an increase of the microhardness observed with a decrease of toughness and resilience properties. The fractography analysis showed typical brittle fracture on the outer diameter of the specimens tested. In the context of GRHYD project, the susceptibility of two brass alloys (CW617N and CW614N) was evaluated in GN + H_2 mixture up to 5 bar pressure under tensile loading on smooth and notched specimens (Briottet *et al.*, 2016). It was found that for the CW617N 20%H_2 was acceptable, Figure 18 and 6%H_2 for the CW614N, Figure 19.

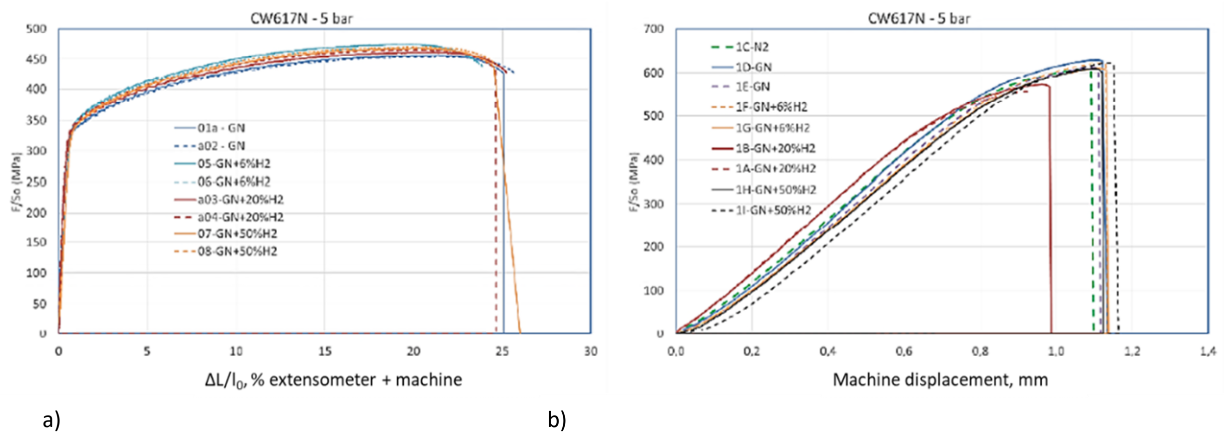

Figure 18 : Tensile curves results for the CW617N on a) smooth and b) notched specimens (Briottet et al., 2016).

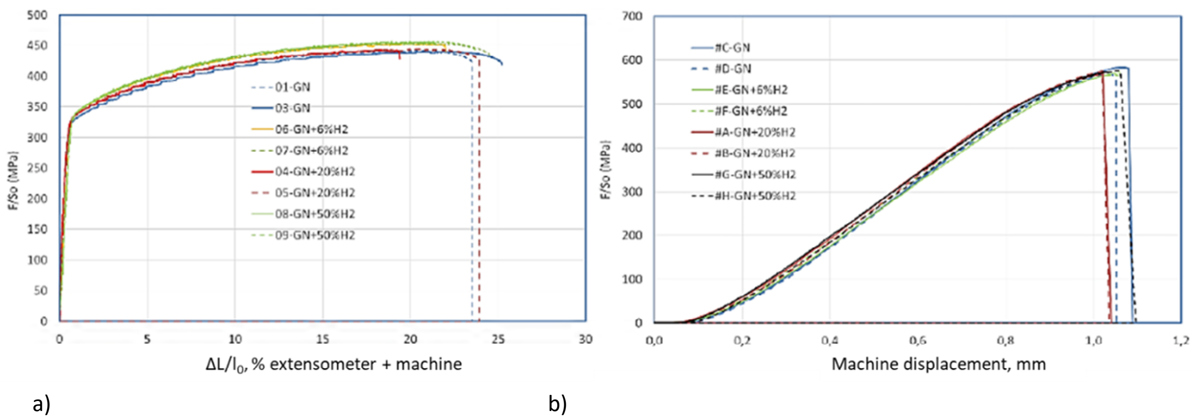

Figure 19 : Tensile curves results for the CW614N on a) smooth and b) notched specimens (Briottet et al., 2016).

2.4.6 Summary and contextual setting

The susceptibility of the main alloys present in the gas distribution networks to HE has been reviewed. Carbon steels were found to be the one with the lowest resistance to HE. However, in the context of investigating the possibility of introducing hydrogen gas in the natural gas distribution network, the operating conditions are much less severe than those that have been investigated. Indeed, carbon steels were tested under 300 bar and 100 bar H_2 pressure and SS under 1 bar with the presence of notches, which increases hydrogen concentration locally. In contrast, operating conditions of the gas network are around 1.03 bar (absolute pressure) at ambient temperature with limited stress concentrations, so not such high HE susceptibility is expected in those conditions.

3 Non-embrittlement concerns induced by the injection of hydrogen in the gas distribution network

3.1 Chemical compatibility

Very few data exist on the chemical compatibility of hydrogen with other materials and it is observed that hydrogen is stable in contact with metals or plastics ("Chemical compatibility guide," 2013). Hydrogen is compatible with polymers or metallic materials: it does not induce their corrosion, as their selective dissolution at room temperature in dry hydrogen gas environment.

PE is a reference of the polymer materials employed by the gas industry and is widely used in gas distribution network. Indeed, it does not have corrosion issues, its maintenance requirements are low, and it is relatively cheap compare to metallic alloys (Iskov et al., 2010).

In the presence of hydrogen, PE presents other advantages, indeed, no deterioration or ageing is observed after long term test: the influence of long term exposure of hydrogen on the mechanical properties and microstructural changes of PE were assessed and no detrimental effects were observed (Castagnet *et al.*, 2010), (Castagnet *et al.*, 2012). Figure 20 shows the evolution of stress-strain curves after 9 to 13 months of exposure to hydrogen gas. Jasionowski *et al.* have investigated the influence of long-term exposure to hydrogen on gas distribution network components. No reduction on performances of the metals and elastomers were observed. However, exposed plastics and adhesive seem to be affected as well as greases which changed in colour and viscosity (Jasionowski *et al.*, 1980).

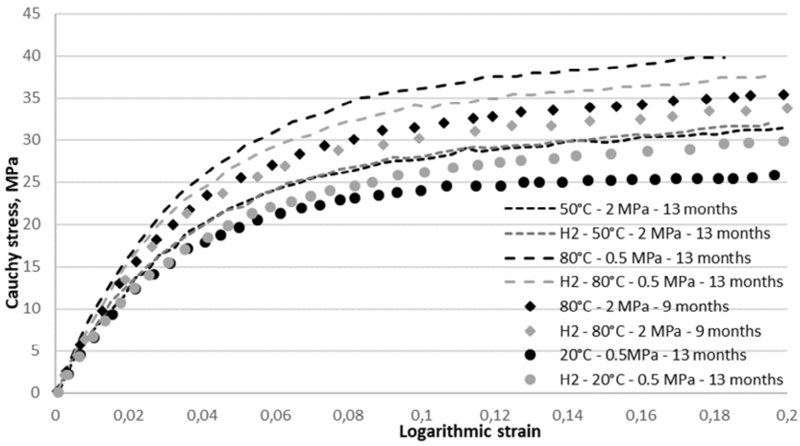

Figure 20 : Stress-strain curves obtained in PE in atmospheric air (0.1 MPa) and in 3 MPa hydrogen after 9 to 13 months of aging at 20°C, 50°C and 80°C (Castagnet et al., 2012).

With the development of fuel cell and hydrogen storage technologies, a lot of data on the behaviour of polymers and elastomers at high hydrogen pressure has been generated. The failure mechanism reported in those materials, and specifically in elastomers, is related to rapid gas decompression. This phenomenon occurs during decompression in components subjected to high pressure once the gas cannot desorb rapidly enough and expands within the material (Castagnet *et al.*, 2018). A brief literature review on this phenomenon is reported here (Barth *et al.*, 2013). The gas pressures addressed by the THyGA project are far too small to induce this type of damage.

3.2 Permeation and leakage

3.2.1 Definition

Hydrogen real leaks are defined as the mobility of dihydrogen and its ability to escape through a small opening, between two pieces of material. Real leaks can be of three types: inboard (flow from the environment to the system, such as contamination), outboard (flow from the system to the environment) and internal (flow across an internal pressure barrier in the system) (*Swagelok Tube Fitters Manual*, n.d.). Those should not be confused with virtual leaks: outgassing (escape of gas from a material) and permeation, which is the ability of a molecule or an atom to diffuse through a bulk material. In metallic materials, as described in the previous section hydrogen dissociates before being adsorbed and absorbed in the metal matrix. In the case of polymers, however, hydrogen diffuses in its molecular form (dihydrogen).

Figure 21 gives a schematic representation of the permeation through polymers and metallic materials as well as an outboard leakage (Barth *et al.*, 2013), (Briottet and Riccetti, 2016). The latter is the one we will be concerned with in the testing part of the project.

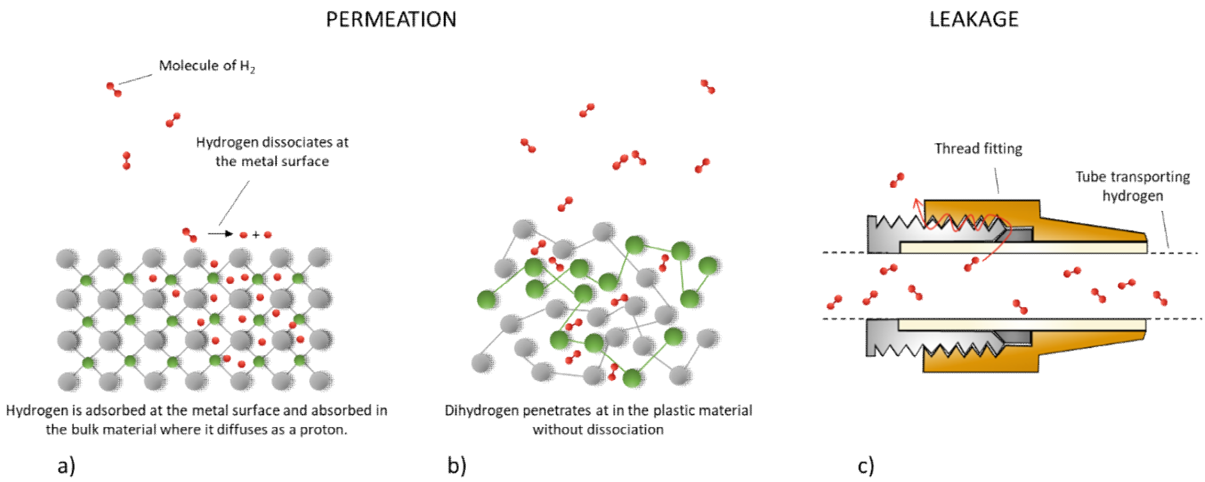

Figure 21 : Schematic representation of permeation in a) a metallic and b) a polymer material and c) leakage through a fitting in hydrogen gas environment.

Assuming that the parameters are known, the flow rate in a system can be estimated using the following formula (*Swagelok Tube Fitters Manual*, n.d.):

$$Q = \frac{\Delta P \times H^3 \times W}{\mu \times L} \qquad \textit{Equation 3}$$

Where, Q is the flow rate of the leak [$m^3.s^{-1}$], ΔP is the pressure drop, W is the circumference of the seal, μ the absolute, or dynamic viscosity [$kg.m^{-1}s^{-1}$], H the height of the gap, and L the length of the leakage path, Figure 22. The dynamic viscosity is different from the cinematic viscosity which is the ratio of the dynamic viscosity of the fluid to its density [$m^2.s^{-1}$].

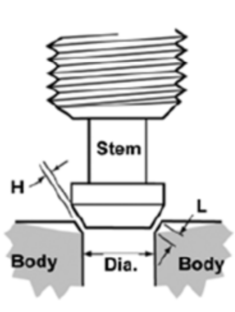

*Figure 22 : Representation of two tubes fitting (*Swagelok Tube Fitters Manual*, n.d.).*

The flow dynamics of gases through tubes or orifices are characterised by the Knudsen number: mean free path over a characteristic dimension (Lafferty, 1998).

$$K_n = \frac{\lambda}{d}$$ *Equation 4*

With λ the mean free path [m], and d the diameter of the pipe or orifice in the system. From this number, three main flow modes can be distinguished depending on the leakage rates ("Leak rates," n.d.) (Lafferty, 1998):

- The free molecular flow standard cubic centimetre (Kn > 0.5): molecular collision with the orifices wall, Figure 23 c).
- The continuum or viscous flow (Kn < 0.01): intermolecular collisions are much more frequent. This flow can be either turbulent, related to a large orifice with high-pressure differential Figure 23 a), or laminar, the flow path is relatively straight along the centre line of the passage Figure 23 b). The flow rate is related to the density or viscosity characteristics of the gas for a turbulent or laminar flow respectively.
- The transitional flow (0.01< Kn < 0.5): defined by the regime in between the free molecular and the continuum flow.

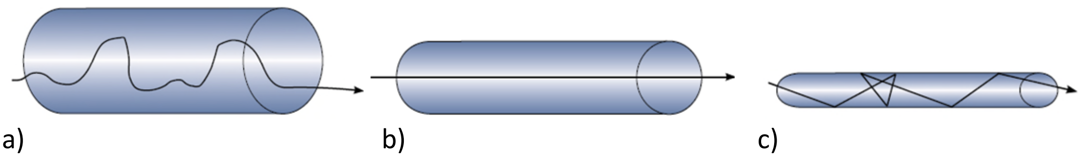

Figure 23: Schematic representation of a molecular path in a a) turbulent flow, b) laminar flow and c) molecular flow ("Leak rates," n.d.).

3.2.2 Hydrogen properties towards leakage

Dihydrogen is one of the smallest molecules, hence its ability to propagate through breaches is higher than methane and propane (Pritchard *et al.*, n.d.). Physical characteristics of methane, propane, helium and hydrogen are given in Table 3.Those values are highly dependent on the leak flow rates of each gas. Laminar leakage and turbulent rates are proportional to the viscosity and the density, respectively. The viscosity represents the internal friction between molecules ("Leak rates," n.d.). Table 3 shows that, in the case of a laminar flow, hydrogen would leak up to 2.8 times faster than methane, on a volumetric basis.

Table 3 : Comparison of the leak characteristics of hydrogen, methane and propane (Leader et al., 2001).

	Hydrogen, H_2	Methane, CH_4	Propane, C_3H_8
Density, Kg,m^{-3}	0.0838	0.6512	1.870
Viscosity, g.cm^{-1}.s^{-1}×10^{-5}	8.9	11.7	8.0
Relative flow rates, volumetric:			
Subsonic flow			
• Laminar flow	1	0.77	1.11
• Turbulent flow	1	0.35	0.21
Sonic flow	1	0.34	0.20

Due to safety concerns, helium (He) is often used instead of hydrogen for leakage simulations of hydrogen testing in order to evaluate the potential presence of leaks (Gupta *et al.*, 2009). This is explained by He being the inert gas with the smallest atom and having a density very close to the hydrogen one, as shown in Table 4. Several works have demonstrated the use of CFD computer models developed with helium experimental data to accurately predict hydrogen temporal and spatial distribution from hydrogen leak in vented or enclosed places (Swain *et al.*, 2002), (Swain *et al.*, 2003), (He *et al.*, 2016). However, in the case of small orifices (10 to 200 µm) it was found that the helium signature test (HST) which is a leak detection technique using helium could under predict hydrogen leakage rates (Lee *et al.*, 2003).

Table 4 : Comparison of hydrogen and helium properties toward leakage ("Leak rates," n.d.).

	Hydrogen, H_2	Helium, He
Density, Kg,m^{-3}	0.0838	0.1634
Viscosity, g.cm^{-1}.s^{-1}×10^{-5}	8.9	19.6
Relative flow rates, volumetric:		
• Laminar flow	2.23	1
• Molecular flow	1.41	1
Atomic weight	1.00797	4.0026

3.2.3 Case of the materials used in gas distribution networks and end-user appliances

Regarding the metallic materials used in gas appliance components, such as carbon steels, stainless steels and copper alloys, the permeation of hydrogen is deemed negligible (Melaina *et al.*, 2013). More of a concern are leakages occurring at seals, fittings, connections and mechanical threads in those materials (Pritchard *et al.*, n.d.). For this reason, it is recommended that welding over threaded connections should always be used when applicable (*Hydrogen transportation pipelines*, 2004).

Polymer materials, such as PE, and elastomer materials however, have a highest permeability to hydrogen that should be understood and taken into account as much as leakage. Polymers have fundamentally different structure than metals. In a very simple manner, polymers can be described as repeated chains liked with each other. Depending on the nature and density of those links polymers are either elastomers, amorphous or semi-crystalline, such as PE. Permeability properties of polymers are dependent on their degree of crystallinity and free-volume fraction which are induced by those links. It was found that hydrogen permeability decreases from elastomers to amorphous and to semi-crystalline polymers (Kane, 2008). Hence, polymers can be engineered in order to decrease their permeability by increasing its degree of crystallinity, within the limits of not changing its mechanical properties.

Important findings, (Alincant et al., 2010; Briottet and Riccetti, 2016; Foulc et al., 2006) are that no incubation time is needed for hydrogen to permeate through PE, which is not the case for methane, and, at room temperature, the permeation coefficient of hydrogen through PE is four to five times higher than methane in a methane plus hydrogen gas mixture, at room temperature. Investigations on the permeability of PE to hydrogen in a CH_4 / H_2 mixture support this finding: the evolution of the permeation of H_2 and CH_4 according to the temperature in the gas mixture is given in Figure 24. Furthermore, it was observed that regardless of the hydrogen concentration, no gas-gas or gas-polymer interactions were detected. The permeation of the two gases is independent of the gas mixture (Klopffer et al., 2007).

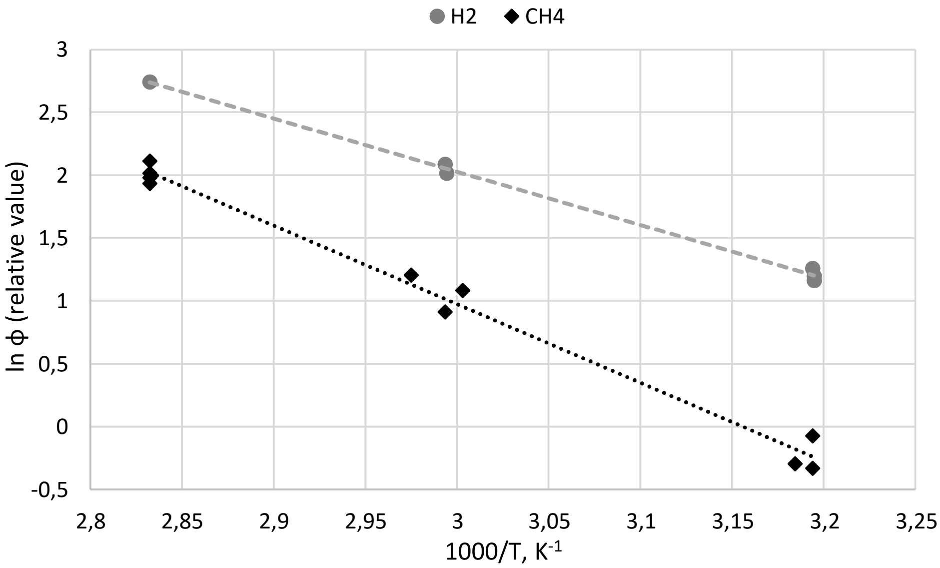

Figure 24 : Evolution of the permeability coefficients of H_2 and CH_4 versus temperature through PE80 exposed to CH_4 / H_2 mixtures (Klopffer et al., 2007).

The permeability, ϕ, is defined by the product of the diffusivity, D [$m^2.s^{-1}$] and the solubility, S [$moleH_2.m^{-3}.MPa^{-1}$], in the case of polymers:

$$\phi = DS \qquad \text{Equation 5}$$

$$[\phi] = \left[\frac{m^2}{s} \times \frac{mole\ H_2}{m^3 MPa}\right] = [\frac{mole\ H_2}{m.s.MPa}] \qquad \text{Equation 6}$$

From the permeability coefficient, it is possible to calculate the quantity of hydrogen that permeates, per unit of time, through a pipe wall for a given material, pipe geometry and hydrogen internal pressure. This quantity, d_{H2} is the flow rate, defined as follow:

$$d_{H_{2,polymer}} = (\frac{\phi \times A}{e_0}) \times P_{H_2} \qquad \text{Equation 7}$$

$$[d_{H_{2,polymer}}] = \left[\frac{molH_2}{m.s.MPa}\right] \times \left[\frac{m^2}{m}\right] \times [MPa] = [\frac{mole_{H_2}}{s}] \qquad \text{Equation 8}$$

The permeability, diffusivity and solubility of LDPE (low density polyethylene) are given on

Table 5. From those data, the flow rate for the geometry of the tube tested in GRHYD project (Briottet and Riccetti, 2016) was calculated and is given in parenthesis

Table 5. The tube geometry was an average diameter of 58.85 × 10^{-3} m, length of 0.143 m, and 6.55× 10^{-3} m thickness with an intern pressure of 0.3 MPa. The results are comparable to the experimental data obtained for a PE tube.

Table 5 : Hydrogen transport properties for LPDE and PE from. (Barth et al., 2013; Pauly, 1999), (Briottet and Riccetti, 2016).

Material	T* (K)	Permeability $\Phi \times 10^{-9}$ $(\frac{molH_2}{m.s.MPa})$	Diffusion coefficient $D \times 10^{-12}$ $(\frac{m^2}{s})$	Solubility S $(\frac{molH_2}{m^3MPa})$	Flow rate $d_{H2,\ polymer} \times 10^{-9}$ $(\frac{molH_2}{s})$	Reference
LPDE	298	3.3	47.4	70.5	(3.99)	(Pauly, 1999)
PE	298				1.9	(Briottet and Riccetti, 2016)

*T = Temperature

The following section aims to give a comparison of the hydrogen losses by permeation through a polymer (LPDE) pipe and a low alloy ferritic steels (Ni-Cr-Mo) pipe for an identical pipe geometry and internal pressure. The pipe dimensions and parameters for the calculation are given in Table 6.

Table 6 : Pipe dimensions and parameters for the calculation

Pipe dimensions

Average diameter, D	20	mm
Thickness of the wall pipe, e_0	1	mm
Length, L	1	m
Permeation area, A	6.28E-02	m^2

Parameters

Relative internal pressure, P	0,1	MPa
Temperature, T	298	K
Gas	100	$\%H_2$

The permeability of the low alloy ferritic steel is calculated using the temperature dependent equation:

$$\phi = \phi_0 \exp\left(\frac{E_a}{RT}\right) \quad \text{Equation 9}$$

$$[\phi_0] = \left[\frac{m^2}{s}\right] \times \left[\frac{mole\ H_2}{m^3\sqrt{MPa}}\right] = \left[\frac{mole\ H_2}{m.s.\sqrt{MPa}}\right] \quad \text{Equation 10}$$

With E_a the activation energy for hydrogen permeation [$J.mol^{-1}$], R the gas constant and T the temperature. The calculation of the flow rate is slightly different for polymers and metals. Indeed, in the case of polymer, $d_{H2polymer}$ is linearly proportional to the pressure. In metals, however, hydrogen dissociates at the metal surface before entering in the crystal lattice, Figure 21. Hence, it is shown that $d_{H,\ metal}$ is proportional to the square root of the inner pressure in the pipe:

$$d_{H,metal} = \left(\frac{\phi \times A}{e_0}\right) \times \sqrt{P_{H_2}} \quad \text{Equation 11}$$

$$[\,d_{H,metal}] = \left[\frac{molH_2}{m.s.\sqrt{MPa}}\right] \times \left[\frac{m^2}{m}\right] \times \left[\sqrt{MPa}\right] = \left[\frac{mole_{H_2}}{s}\right] \quad \text{Equation 12}$$

From these equations, it is possible to estimate the linear flow rate of hydrogen, d_{lin}, lost by permeation through a specific geometry and pipe material, according to the inner pressure of the pipe:

$$d_{lin,polymer} = \frac{d_{H_2}}{L \times P_{H_2}};\ [d_{lin,polymer}] = \frac{[\frac{mole_{H_2}}{s}]}{[m \times MPa]} = \left[\frac{mole_{H_2}}{m \times MPa \times s}\right] \quad \text{Equation 13}$$

$$d_{lin,metal} = \frac{d_H}{L\times\sqrt{P_{H2}}};\ [d_{lin,metal}] = \frac{[\frac{mole_{H_2}}{s}]}{[m\times\sqrt{MPa}]} = [\frac{mole_{H_2}}{m\times\sqrt{MPa}\times s}]$$ *Equation 14*

Table 7 : Permeability coefficients for the Ni-Cr-Mo steel and LPDE (San Marchi and Somerday, 2012) and calculation of the resulting flow loss through the pipe of dimensions given in Table 6.

	Low alloy ferritic steel: Ni-Cr-Mo	**LPDE**
E_ϕ, $J.mol^{-1}$	39,300	
ϕ_0, $molH_2.m^{-1}s^{-1}.MPa^{-0.5}$ (metals), $molH_2.m^{-1}s^{-1}.MPa$ (polymer)	0.00015	
ϕ, $molH_2.m^{-1}s^{-1}.MPa^{-0.5}$ (metals), $molH_2.m^{-1}s^{-1}.MPa$ (polymer)	1.94E-11	3.3E-09
d_{H2}, $molH_2.s^{-1}$	3.85E-10	2.07E-08
d_{lin}, $molH_2.m^{-1}.MPa^{-1/2}s^{-1}$ (metals), $molH_2.m^{-1}s^{-1}.MPa$ (polymer)	1.22E-09	2.07E-07

From this calculation, it is found that the flow of hydrogen per seconds according to the inside pressure of the pipe was two orders of magnitude lower for the Ni-Cr-Mo low alloy steel than for the LPDE at 298 K. This is in agreement with Jasionowski *et al.* (Jasionowski *et al.*, 1980) work in which long term tightness testing on two loops representative of gas distribution networks: an industrial and a domestic one, in natural gas and hydrogen were performed. The volumetric leak ratio of hydrogen to NG of the entire sets up were 3 for the domestic loop and 3.35 for the industrial installation. The individual leak rates for the individual components in NG and hydrogen were encapsulated into Plexiglas container in order to measure their individual leakage flow rates. Results are given in Table 8, it is clear that metallic components have better tightness properties than polymer parts.

Table 8 : Leak rates for enclosed components tested in hydrogen and natural gas (Jasionowski et al., 1980).

Enclosure No.	Component	NG[a] Test duration (hr) 352	457	760	NG Avg.	H_2 test duration (hr) 720	933	1610	H_2 avg.	Leak ratio H_2 avg.
3	2-in. hydraulically applied coupling; rubber seal on steel pipe	0.08	0.13	0.07	0.09	0.37	0.36	0.33	0.35	3.9
7	2-in. coupling with 3-bolt construction; rubber seal on steel pipe	0.05	0.08	0.03	0.05	0.24	0.21	0.23	0.23	4.6
9	2-in. weld joint; steel pipe	0	0	0	0	0	0	0	0	0
11	2-in. hydraulically applied transition coupling; rubber seal on polyethylene and steel pipe	0.74	0.94	0.75	0.80	4.60	3.43	1.78	2.87	3.83
10	2-in. pipe thread coupling;[b] steel pipe	—	1,100	4,150	—	—	4,900	—	—	4.3[c]
1	2-in. insulating joint; steel[b] pipe	<10	<10	<10	<10	<10	<10	<10	<10	—
2	2-in. compression coupling;[b] steel pipe	<10	<10	<10	<10	<10	<10	<10	<10	—
4	2-in. flanged joint with[b] asbestos gasket	<10	<10	<10	<10	<10	<10	<10	<10	—
5	Residential service regulator[b]	<10	<10	<10	<10	<10	<10	<10	<10	—
6	Residential meter[b]	<10	<10	<10	<10	<10	<10	<10	<10	—
8	2-in. insulating union with[b] threaded ends; steel pipe	<10	<10	<10	<10	<10	<10	<10	<10	—
12	Lubricated plug valve[b] (leakage from grease fitting)	—	—	—	—	—	—	—	67,000	67,000

Leak rate (cc/24-hr day)

[a] NG = natural gas.
[b] Instantaneous leak rate by the bubble piston method; 10 cm^3/day minimum detectable leakage. All other measurements made by gas analysis.
[c] Based on initial NG leak rate; leakage increased during operations.

In NATURALHY project, the gas loss rate, through PE 80 32 mm diameter pipes, for the gas mixture CH_4 / H_2 was estimated according to the hydrogen content at 4 bar, 8 bar and 12 bar (Melaina et al., 2013), the results are given in Table 9. It was found that gas losses increased with the hydrogen content in the mixture CH_4 / H_2, deriving from the highest permeability of hydrogen compared to methane. From those results, it was concluded that the gas losses were negligible in an economical point of view.

Table 9 : Calculated gas loss from a 32 mm diameter PE 80 pipe under the pressure of 4, 8 and 12 bar (Melaina et al., 2013).

Gas	Gas Pressure (bar)	Time-Lag (day)		Gas Loss ($m^3.km^{-1}.year^{-1}$)		
		CH_4	H_2	CH_4	H_2	Total
Pure CH_4	4	6.46	NA	0.95	0.00	0.95
90% CH_4 + 10% H_2	4	4.31	0.00	0.46	0.19	0.64
	8	6.39	0.00	1.18	0.55	1.73
	12	5.69	0.00	1.79	0.85	2.65

3.2.4 Acceptance criteria for gas distribution network components

Table 10 gives applied gas flow rates acceptance for some components of the gas distribution network. Depending on the connections type, some leakage can be accepted: 0.04 $dm^3.h^{-1}$ for pressure regulator and safety devices for gas appliances and 0.01 $dm^3.h^{-1}$ for connections of gas appliances. Hence, leakage are expected, and will be measured in WP3 Task 3.2.3: Leakage tests on indoor installation (long term), see chapter 4.

Table 10: Current flow rates requirements for the components of gas distribution network.

Standards	Acceptance criterion $dm^3.h^{-1}$	Comments
DVGW G 5614 : Permanent pipe connections for metal gas pipes; press-fitted connectors	0	Tightness: test related to DIN EN 12266-1, with the test medium air at room temperature; leakage rate "A"
Separable unthreaded pipe connections for metal gas pipe - Part 1: Connections for pipes with smooth ends	0	See Table 01 – leakage rate "A" No Leakage allowed for minimum 10 min
DVGW G 5628 : Installation Systems for Gas Installation inside Buildings, consisting of Multi-Layer Pipes and their corresponding Fittings, for an Operating Pressure less than or equal to 100 mbar;	0	
DIN EN 88-1: Pressure regulators and associated safety devices for gas appliances – Part 1: Pressure regulators for inlet pressures up to and including 50 kPa	0.04	Tests and criteria according to DIN EN 13611, Safety and control devices for burners and fuel devices for gaseous and / or liquid fuels - General requirements - External tightness at 150 mbar (max.)
DIN EN 3383-1 : Connection of gas appliances – Part 1: Gas connection valves, safety hose assemblies	0.01	Type H - The connection is tested under water with air or nitrogen and an internal pressure of 20 mbar and 150 mbar, the leakage rate must not exceed 10 $cm^3.h^{-1}$ TYPE N - The connection is tested under water with air or nitrogen and an internal pressure of 20 mbar and 150 mbar, the leakage rate must not exceed 10 $cm^3.h^{-1}$

4 Experimental method for the leakage tests on indoor installation (Task 3.2.3)

4.1 Objective

The objective of the Task 3.2.3 is to evaluate the tightness of the components located on the gas line within the building from Germany, Denmark, Belgium and France. Ideally, the components tested should be the one used currently on the network. In addition, appliance components (oven and hob from Electrolux, boiler from BDR) will also be tested for completeness: test of the gas distribution line from the gas meter to the end user.

4.2 Set up

Two methods are used to measure the potential leakage. The first one is static: the installation is closed and the pressure is monitored, a pressure drop indicates the presence of a leak. The second one is dynamic: a gas flux is inserted in the installation to reach a determined pressure level. An increase in flow once the pressure level is reached will indicate a leak. In this test, the two methods are used alternatively. The first method is used over the whole testing period (over 6 months) and for short duration it is interrupted to apply the second method (several hours).

Figure 25 is a representation of the experimental set-up. The components are taken from the installation without being dismounted in order to be as closed as possible from the operating conditions. They are distributed on the lines according to the material of their previous installation (copper, steel, polymer …) to form 5 independent lines. On each line the components are connected in series, by welding if possible, in order to reduce potential leakage and all the lines are closed by manual valves at the entrance (V_1, V_2, V_3, V_4, V_5) and exit (V_a, V_b, V_c, V_d, V_e); the 5 lines are connected to the same manifold. Pressure gauges are measuring the gas pressure of each line, which are recorded using a data acquisition system. Two gas bottles one of nitrogen and one of the chosen gas mixture are used to fill in the lines. A flow meter is positioned on the main manifold.

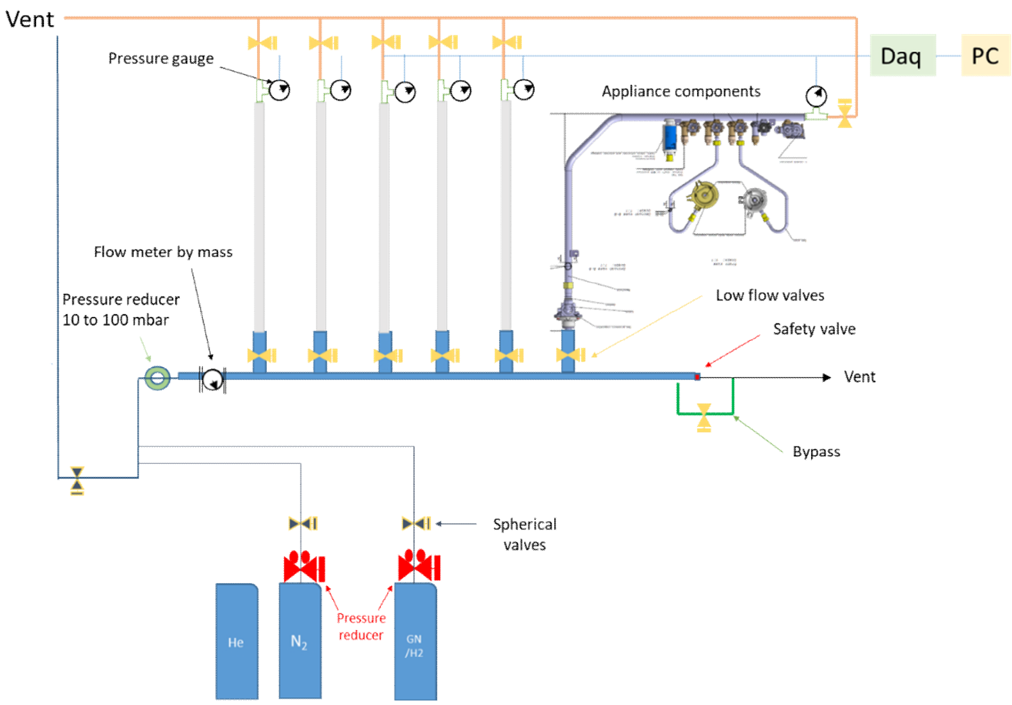

Figure 25 : Schematic representation of the leakage test set up.

4.3 Procedure

<u>Static test:</u>

- The lines are first purged with N_2.
- The gas mixture is circulated in all the lines, making sure no N_2 is left.
- The exit valves are closed and lines are filled with the gas mixture up to 30 mbar.
- Once the pressure is reached, the entrance valves are closed and measure of the pressure is recorded (several months).
- If a leak is detected by a pressure drop the corresponding line is emptied from the gas mixture and filled with He. The location of the leak is determined using a He gas detector.

The parameters used for this test are the following:

- Gas: CH_4 + 60% H_2.
- Pressure in the lines: 30 mbar.
- Duration of the test: several months.
- Monitoring of the pressure in the lines.

<u>Dynamic test:</u>

- Alternatively, the gas flow is measured in each line (some hours).
- If a leak is detected by an increasing of gas flow, the corresponding line is emptied from the gas mixture and filled with He. The location of the leak is determined using a He gas detector.

The parameters used for the test are the following:

- Gas: CH_4 + 60% H_2
- Pressure in the lines: 30 mbar
- Duration of the test: several hours
- Measuring the flow of each line alternatively

5 Conclusion

This literature survey aimed to review non-combustion concerns related to the introduction of NG / H_2 gas mixture in the gas distribution network within buildings i.e. operating pressures between 30 to 50 mbar. Four mechanisms of HE on metallic materials were described with a focus on HE of the main metallic materials of the gas distribution network. The chemical compatibility with hydrogen of the materials present in the gas distribution network and specifically polymers, was addressed. The last part concerned tightness issues that could result from the introduction of hydrogen in the gas network in terms of leakage and permeation.

- From the HE results presented, the partial pressures of the operating gas distribution are low and it is assumed that a gas mixture composed of NG and up to 50% H_2 should not be problematic for any of the metallic materials employed in gas distribution system, unless high mechanical stress / strain and high stress concentrations are applied.
- Furthermore, investigation on chemical compatibility have shown that polymer materials, and specifically PE, are not subjected to deterioration after long term exposure in dihydrogen.
- In terms of leakage, the propensity of hydrogen to leak was also considered, hydrogen leaks 2.5 times quicker than methane, due to its different physical properties.
- The permeability of hydrogen was also reviewed, if it is insignificant in metals, it was considered for PE, but in the operations conditions of this work the gas losses were assumed to be negligible.

This theoretical report on material deterioration, chemical compatibility and leakage concerns coming with the introduction of NG / H_2 mixture in the gas distribution network sets the basis for the upcoming experimental work where the tightness of gas distribution network components will be investigated (Task 3.2.3, WP3). In addition, tightness of typical components that connect end-user appliances to the local distribution line shall be evaluated as well.

6 List of Illustrations

7 List of tables

8 List of references

Abraham, D.P., Altstetter, C.J., 1995. Hydrogen-enhanced localization of plasticity in an austenitic stainless steel. MMTA 26, 2859–2871. https://doi.org/10.1007/BF02669644

Alincant, D., Berne, Ph., Demiaux, D., Morel, B., Pocachard, J., 2010. Perméation de l'hydrogène à travers différents types de polymères : Caractérisation et évolution en vieillissement. Projet PolHYtube – Tâches 1, 3 et 4.

Ambat, R., Dwarakadasa, E.S., 1996. Effect of hydrogen in aluminium and aluminium alloys: a review. Bull. Mater. Sci. 19, 103–114. https://doi.org/10.1007/BF02744792

Barth, R.R., Simmons, K.L., San Marchi, C.W., 2013. Polymers for hydrogen infrastructure and vehicle fuel systems (No. SAND2013-8904, 1104755). https://doi.org/10.2172/1104755

Barthelemy, H., 2006. Compatibility of metallic materials with hydrogen review of the present knowledge.

Birenis, D., Ogawa, Y., Matsunaga, H., Takakuwa, O., Yamabe, J., Prytz, O., Thogersen, A., 2018. Interpretation of hydrogen-assisted fatigue crack propagation in BCC iron based on dislocation structure evolution around the crack wake | Elsevier Enhanced Reader. Acta Materialia. https://doi.org/10.1016/j.actamat.2018.06.041

Birnbaum, H.K., 1979. Hydrogen Related Failure Mechanisms in Metals (No. N00014-75- C–1012). Department of Metallurgy and Mining Engineering, University of Illinois at Urbana- Champaign Urbana, Illinois 61801 U.S.A.

Birnbaum, H.K., Sofronis, P., 1994. Hydrogen-enhanced localized plasticity—a mechanism for hydrogen-related fracture. Materials Science and Engineering: A 176, 191–202.

Birnbaum, H.K., Wert, C.A., 1972. Diffusion of hydrogen in metals.

Bond, G.M., Robertson, I.M., Birnbaum, H.K., 1988. Effects of hydrogen on deformation and fracture processes in high-purity aluminium. Acta Metallurgica 36, 2193–2197. https://doi.org/10.1016/0001-6160(88)90320-3

Brass, A.-M., Chêne, J., Coudreuse, L., 2000. Fragilisation des aciers par l'hydrogène : étude et prévention.

Briottet, L., Batisse, R., de Dinechin, G., Langlois, P., Thiers, L., 2012. Recommendations on X80 steel for the design of hydrogen gas transmission pipelines. International Journal of Hydrogen Energy 37, 9423–9430. https://doi.org/10.1016/j.ijhydene.2012.02.009

Briottet, L., Ez-Zaki, H., 2018. Influence of Hydrogen and Oxygen Impurity Content in a Natural Gas / Hydrogen Blend on the Toughness of an API X70 Steel, in: Volume 6B: Materials and Fabrication. Presented at the ASME 2018 Pressure Vessels and Piping Conference, American Society of Mechanical Engineers, Prague, Czech Republic. https://doi.org/10.1115/PVP2018-84658

Briottet, L., Portra, T., 2017. Evaluation de la sensibilité à la fragilisation par l'hydrogène de tubes de cuivre dans le cadre du projet GRHYD Tâche WP5-Matériels de réseau et compresseurs (Rapport technique No. DTBH/LV/2017/092). Liten, CEA, Grenoble.

Briottet, L., Portra, T., Mollard, C., 2016. Evaluation de la sensibilité à la frailiation par l'hydrogène d'alliages métalliques dans le cadre du projet GRHYD (No. DTBH/RT/2016/220).

Briottet, L., Riccetti, B., 2016. Permeation de l'hydrogene dans une canalisation en polyethylene,Tâche WP5-Matériels de réseau et compresseurs (Rapport technique No. DTBH/RT/2016/065). Liten, CEA, Grenoble.

Bruzzoni, P., Riecke, E., 1994. On the mechanism of hydrogen transport through the passive oxide film on iron. Corrosion Science 36, 1597–1614. https://doi.org/10.1016/0010-938X(94)90056-6

Capelle, J., Gilgert, J., Dmytrakh, I., Pluvinage, G., 2008. Sensitivity of pipelines with steel API X52 to hydrogen embrittlement. International Journal of Hydrogen Energy 33, 7630–7641. https://doi.org/10.1016/j.ijhydene.2008.09.020

Castagnet, S., Grandidier, J.-C., Comyn, M., Benoît, G., 2012. Effect of long-term hydrogen exposure on the mechanical properties of polymers used for pipes and tested in pressurized hydrogen. International Journal of Pressure Vessels and Piping 89, 203–209. https://doi.org/10.1016/j.ijpvp.2011.11.008

Castagnet, S., Grandidier, J.C., Comyn, M., Benoit, G., 2010. Hydrogen influence on the tensile properties of mono and multi-layer polymers for gas distribution | Elsevier Enhanced Reader 7633–7640. https://doi.org/10.1016/j.ijhydene.2010.04.155

Castagnet, S., Mellier, D., Nait-Ali, A., Benoit, G., 2018. In-situ X-ray computed tomography of decompression failure in a rubber exposed to high-pressure gas. Polymer Testing 70, 255–262. https://doi.org/10.1016/j.polymertesting.2018.07.017

Chemical compatibility guide, 2013.

Dadfarnia, M., Martin, M.L., Nagao, A., Sofronis, P., Robertson, I.M., 2015a. Modeling hydrogen transport by dislocations. Journal of the Mechanics and Physics of Solids 78, 511–525. https://doi.org/10.1016/j.jmps.2015.03.002

Dadfarnia, M., Nagao, A., Wang, S., Martin, M.L., Somerday, B.P., Sofronis, P., 2015b. Recent advances on hydrogen embrittlement of structural materials. Int J Fract 196, 223–243. https://doi.org/10.1007/s10704-015-0068-4

Dey, S., Chattoraj, I., 2016. Interaction of strain rate and hydrogen input on the embrittlement of 7075 T6 Aluminum alloy. Materials Science and Engineering: A 661, 168–178. https://doi.org/10.1016/j.msea.2016.03.010

Djukic, M.B., Zeravcic, V.S., Bakic, G., Sedmak, A., Rajicic, B., 2014. Hydrogen Embrittlement of Low Carbon Structural Steel. Procedia Materials Science 3, 1167–1172. https://doi.org/10.1016/j.mspro.2014.06.190

Eliezer, D., Chakrapani, D.G., Altstetter, C.J., Pugh, E.N., 1979. The influence of austenite stability on the hydrogen embrittlement and stress- corrosion cracking of stainless steel. MTA 10, 935–941. https://doi.org/10.1007/BF02658313

Ez-Zaki, H., Briottet, L., Christien, F., Bosch, C., Levasseur, O., Leriverain, A., Bertin, M., 2018. La fragilisation par l'hydrogène gazeux de l'acier L485 MB pour le transport de mélange GN/H2 8.

FD E29-649 Bouteilles à gaz transportables - fragilisation par l'hydrogène des aciers, 2016.

Foulc, M.-P., Nony, F., Mazabraud, P., Berne, P., Flaconneche, B., Pimenta, G.F., Syring, G.M., Alliat, I., 2006. Durability and transport properties of polyethylene pipes for distributing mixtures of hydrogen and natural gas 6.

Fukai, Y., 2005. The metal-hydrogen system: basic bulk properties, 2nd rev. and updated ed. ed, Springer series in materials science. Springer, Berlin ; New York.

Fukuyama, S., Yokogawa, K., 1990. Prevention of hydrogen environemntal assisted crack growth of 2.25Cr-1Mo steel by gaseous inhibitors 914–923.

Gupta, S., Brinster, J., Studer, E., Tkatschenko, I., 2009. Hydrogen related risks within a private garage: Concentration measurements in a realistic full scale experimental facility. International Journal of Hydrogen Energy 34, 5902–5911. https://doi.org/10.1016/j.ijhydene.2009.03.026

He, J., Kokgil, E., Wang, L. (Leon), Ng, H.D., 2016. Assessment of similarity relations using helium for prediction of hydrogen dispersion and safety in an enclosure. International Journal of Hydrogen Energy 41, 15388–15398. https://doi.org/10.1016/j.ijhydene.2016.07.033

Hydrogen transportation pipelines (Rapport technique No. IGC Doc 121/04/E), 2004. . European Industrial Gases Association.

Iskov, H., Backman, M., Nielsen, H.P., 2010. Field Test of Hydrogen in the Natural Gas Grid, in: Schriften Des Forschungszentrums Jülich Reihe Energie & Umwelt. Forschungszentrum, IEF-3, Jülich.

Jasionowski, W., Pangborn, J., Johnson, D., 1980. Gas distribution equipment in hydrogen service. International Journal of Hydrogen Energy 5, 323–336. https://doi.org/10.1016/0360-3199(80)90076-2

Jewett, R.P., Walter, R.J., Chandler, W.T., Frohmberg, R.P., 1973. Hydrogen environment embrittlement of metals (No. NASA CR-2163). Washington D.C.

Johnson, B., 1874. On some remarkable changes produced in iron and steel by the action of hydrogen and acids 12.

Kamoutsi, H., Haidemenopoulos, G.N., Bontozoglou, V., Pantelakis, S., 2006. Corrosion-induced hydrogen embrittlement in aluminum alloy 2024. Corrosion Science 48, 1209–1224. https://doi.org/10.1016/j.corsci.2005.05.015

Kane, M.C., 2008. Permeability, Solubility, and interaction of Hydrogen in Polymers- An assessment of materials for hydrogen transport (Rapport technique No. WSRC-STI-2008-00009). Savannah River National Laboratory, Aiken, SC 29808.

Kirchheim, R., 1986. Interaction of hydrogen with external stress fields. Acta Metallurgica 34, 37–42.

Klopffer, M.H., Flaconneche, B., Odru, P., 2007. Transport properties of gas mixtures through polyethylene. Plastics, Rubber and Composites 36, 184–189. https://doi.org/10.1179/174328907X191350

Komoda, R., Kubota, M., Staykov, A., Ginet, P., Barbier, F., Furtado, J., 2019. Inhibitory effect of oxygen on hydrogen-induced fracture of A333 pipe steel. Fatigue Fract Eng Mater Struct 42, 1387–1401. https://doi.org/10.1111/ffe.12994

Krom, A.H.M., 1998. Numercial modelling of hydrogen transport in steel. Delft.

Krom, A.H.M., Koers, R.W.J., Bakker, A., 1999. Hydrogen transport near a blunting crack tip. Journal of the Mechanics and Physics of Solids 47, 971–992. https://doi.org/10.1016/S0022-5096(98)00064-7

Lafferty, J.M. (Ed.), 1998. Flow gases through tubes and orifices, in: Foundations of Vacuum Science and Technology. Wiley, New York.

Leader, W., Partners, W., Huld, T., 2001. Compilation of Existing Safety Data on Hydrogen and Comparative Fuels. Report Title 15.

Leak rates, n.d.

Lee, I.D., Smith, O.I., Karagozian, A.R., 2003. Hydrogen and Helium Leak Rates from Micromachined Orifices. AIAA Journal 41, 457–464. https://doi.org/10.2514/2.1967

Legrand, E., Bouhattate, J., Feaugas, X., Garmestani, H., 2012. Computational analysis of geometrical factors affecting experimental data extracted from hydrogen permeation tests: II – Consequences of trapping and an oxide layer. International Journal of Hydrogen Energy 37, 13574–13582. https://doi.org/10.1016/j.ijhydene.2012.06.043

Li, X., Zhang, J., Fu, Q., Akiyama, E., Song, X., Wang, Y., Li, Q., Zou, N., 2018. Tensile mechanical properties and fracture behaviors of nickel-based superalloy 718 in the presence of hydrogen. International Journal of Hydrogen Energy 43, 20118–20132. https://doi.org/10.1016/j.ijhydene.2018.08.179

Liu, M.A., Rivera-Díaz-del-Castillo, P.E.J., Barraza-Fierro, J.I., Castaneda, H., Srivastava, A., 2019. Microstructural influence on hydrogen permeation and trapping in steels. Materials & Design 167, 107605. https://doi.org/10.1016/j.matdes.2019.107605

Liu, Q., Yang, S., Shen, L., Zhou, Q., Li, J., Su, Y., Qiao, L., Yan, Y., 2020. The effect of hydrogen concentration on the fracture surface of medium Mn steels. Engineering Failure Analysis 108, 104263. https://doi.org/10.1016/j.engfailanal.2019.104263

Louthan, M.R., Caskey, J.R., 1976. Hydrogen transport and embrittlement in structural metals. Northern Ireland 15.

Louthan, M.R., Caskey, J.R., Donovan, J.A., Rawl, D.E., 1972. Hydrogen embrittlement of metals. Materials Science and Engineering 357–368.

Luppo, M.I., Ovejero-Garcia, J., 1991. The influence of microstructure on the trapping and diffusion of hydrogen in a low carbon steel. Corrosion Science 32, 1125–1136. https://doi.org/10.1016/0010-938X(91)90097-9

Lynch, S., 2012. Hydrogen embrittlement phenomena and mechanisms. Corrosion Reviews 30. https://doi.org/10.1515/corrrev-2012-0502

Lynch, S.P., 2011. Hydrogen embrittlement (HE) phenomena and mechanisms, in: Stress Corrosion Cracking. Elsevier, pp. 90–130. https://doi.org/10.1533/9780857093769.1.90

Marrow, T.J., Cotterill, P.J., King, J.E., 1992. Temperature effects on the mechanism of time independent hydrogen assisted fatigue crack propagation in steels. Acta metallurgica et materialia 40, 2059–2068.

Mechanics - Microstructure - Corrosion Coupling - 1st Edition, 2019. . Christine Blanc, Isabelle Aubert.

Melaina, M.W., Antonia, O., Penev, M., 2013. Blending Hydrogen into Natural Gas Pipeline Networks: A Review of Key Issues. Renewable Energy 131.

Nagao, A., Martin, M.L., Dadfarnia, M., Sofronis, P., Robertson, I.M., 2014. The effect of nanosized (Ti,Mo)C precipitates on hydrogen embrittlement of tempered lath martensitic steel. Acta Materialia 74, 244–254. https://doi.org/10.1016/j.actamat.2014.04.051

Nagumo, M., 2004. Hydrogen related failure of steels – a new aspect. Materials Science and Technology 20, 940–950. https://doi.org/10.1179/026708304225019687

Nguyen, T.T., Park, J., Kim, W.S., Nahm, S.H., Beak, U.B., 2020. Effect of low partial hydrogen in a mixture with methane on the mechanical properties of X70 pipeline steel. International Journal of Hydrogen Energy 45, 2368–2381. https://doi.org/10.1016/j.ijhydene.2019.11.013

Nieh, T.G., Nix, W.D., 1980. The formation of water vapor bubbles in copper and their effect on intergranular creep fracture. Acta Metallurgica 28, 557–566. https://doi.org/10.1016/0001-6160(80)90122-4

Oriani, R.A., Josephic, P.H., 1974. Equilibrium aspects of hydrogen-induced cracking of steels. Acta Metallurgica 22, 1065–1074.

Panagopoulos, C., Papapanayiotou, P., 1995. The influence of cathodic hydrogen charging on the mechanical behaviour of Al-4Zn-1Mg alloy. Journal of Materials Science 30, 3449–3456. https://doi.org/10.1007/BF00349893

Panagopoulos, C.N., El-Amoush, A.S., Georgarakis, K.G., 2005. The effect of hydrogen charging on the mechanical behaviour of α-brass. Journal of Alloys and Compounds 392, 159–164. https://doi.org/10.1016/j.jallcom.2004.09.011

Pauly, S., 1999. Permeability and diffusion data, in: Polymer Handbook. J. Brandrul, EH Immergut and EA Grulke, New York.

Perng, T.P., Altstetter, C.J., 1987. Comparison of hydrogen gas embrittlement of austenitic and ferritic stainless steels. MTA 18, 123–134. https://doi.org/10.1007/BF02646229

Pfeil, L.B., 1926. The effect of occluded hydrogen on the tensile strength of iron 182–195.

Pritchard, D.K., Royle, M., Willoughby, D., n.d. Guidance for hydrogen and fuel cell stationary applications 74.

Robertson, I.M., Sofronis, P., Nagao, A., Martin, M.L., Wang, S., Gross, D.W., Nygren, K.E., 2015. Hydrogen Embrittlement Understood. Metall and Mat Trans A 46, 2323–2341. https://doi.org/10.1007/s11661-015-2836-1

San Marchi, C.W., Somerday, B.P., 2012. Technical reference for hydrogen compatibility of materials. (No. SAND2012-7321, 1055634). https://doi.org/10.2172/1055634

Scully, J.R., Young, G.A., Smith, S.W., 2012. Hydrogen embrittlement of aluminum and aluminum-based alloys, in: Gaseous Hydrogen Embrittlement of Materials in Energy Technologies. Elsevier, pp. 707–768. https://doi.org/10.1533/9780857093899.3.707

Shinko, T., Hénaff, G., Halm, D., Benoit, G., Bilotta, G., Arzaghi, M., 2019. Hydrogen-affected fatigue crack propagation at various loading frequencies and gaseous hydrogen pressures in commercially pure iron. International Journal of Fatigue 121, 197–207. https://doi.org/10.1016/j.ijfatigue.2018.12.009

Song, J., Soare, M., Curtin, W.A., 2010. Testing continuum concepts for hydrogen embrittlement in metals using atomistics. Modelling Simul. Mater. Sci. Eng. 18, 045003. https://doi.org/10.1088/0965-0393/18/4/045003

Swagelok Tube Fitters Manual, n.d. . Solon Ohio.

Swain, M., Filoso, P., Grilliot, E., Swain, M., 2003. Hydrogen leakage into simple geometric enclosures. International Journal of Hydrogen Energy 28, 229–248. https://doi.org/10.1016/S0360-3199(02)00048-4

Swain, M.R., Grilliot, E.S., Swain, M.N., 2002. The Application of a Hydrogen Risk Assessment Method to Vented Spaces, in: Grégoire Padró, C.E., Lau, F. (Eds.), Advances in Hydrogen Energy. Kluwer Academic Publishers, Boston, pp. 163–173. https://doi.org/10.1007/0-306-46922-7_13

Takai, K., Shoda, H., Suzuki, H., Nagumo, M., 2008. Lattice defects dominating hydrogen-related failure of metals. Acta Materialia 56, 5158–5167. https://doi.org/10.1016/j.actamat.2008.06.031

Thibaut, O., 2020. Discussion on gas appliances components to test.

Vandervoort, R.R., Raymond, E.L., 1976. Tensile properties of welded or sensitized 316 stainless steel in high-pressure hydrogen gas. United States.

Wang, R., 2009. Effects of hydrogen on the fracture toughness of a X70 pipeline steel. Corrosion Science 51, 2803–2810. https://doi.org/10.1016/j.corsci.2009.07.013

Wang, S., Martin, M.L., Robertson, I.M., Sofronis, P., 2015. Unpublished work.

Yang, Y., Shi, L., Xu, Z., Lu, H., Chen, X., Wang, X., 2015. Fracture toughness of the materials in welded joint of X80 pipeline steel. Engineering Fracture Mechanics 148, 337–349. https://doi.org/10.1016/j.engfracmech.2015.07.061